12-2020

Utilization of Raman Spectroscopic Techniques for Forensic Science Applications

Alyssa Rose Daniel
adanie36@vols.utk.edu

Recommended Citation

Daniel, Alyssa Rose, "Utilization of Raman Spectroscopic Techniques for Forensic Science Applications. " Master's Thesis, University of Tennessee, 2020.
https://trace.tennessee.edu/utk_gradthes/5836

To the Graduate Council:

I am submitting herewith a thesis written by Alyssa Rose Daniel entitled "Utilization of Raman Spectroscopic Techniques for Forensic Science Applications." I have examined the final electronic copy of this thesis for form and content and recommend that it be accepted in partial fulfillment of the requirements for the degree of Master of Science, with a major in Chemistry.

Bhavya Sharma, Major Professor

We have read this thesis and recommend its acceptance:

Shawn R. Campagna, Ampofo K. Darko

Accepted for the Council:
Dixie L. Thompson

Vice Provost and Dean of the Graduate School

(Original signatures are on file with official student records.)

Utilization of Raman Spectroscopic Techniques for Forensic Science Applications

A Thesis Presented for the
Master of Science
Degree
The University of Tennessee, Knoxville

Alyssa Rose Daniel
December 2020

DEDICATION

This work is dedicated to my loving parents, who have supported me through the good and bad times. This is also dedicated to my siblings, who have always been there for support whenever I have needed them.

ACKNOWLEDGEMENTS

Firstly, thank you to my advisor Dr. Bhavya Sharma. Your unwavering support and guidance through the last three years has been nothing short of extraordinary. I want to express my deepest gratitude for your patience, understanding, and kind-heartedness through my time here at UTK. I am so proud to have contributed to the Sharma Group, and I am forever thankful for the knowledge I attained while working under your direction.

Secondly, thank you to the Sharma group members past and present. Amber, Josh, Grace, Avery, Paula thank you for always being there to answer questions, give your support, and for making our science fun. Taylor, James, and Sarah, thank you for your help in collecting data. I am grateful to every one of you.

Lastly, thank you to my committee members, Dr. Shawn Campagna, Dr. Dawnie Steadman, and Dr. Ampofo Darko for your time, insight, and encouragement.

ABSTRACT

In the field of forensic science, it is important to have reliable, accurate, and nondestructive testing methods for evidence collection and testing. Current methods, such as gas chromatography-mass spectrometry (GC-MS) and high-performance liquid chromatography (HPLC), are destructive to evidence and require lengthy sample preparation. Because of its nondestructive nature, specificity, and portability, Raman spectroscopy has been increasingly improving forensic science. The goal of this work is to expand on the growing pool of knowledge of forensics related Raman applications.

One problem that has plagued forensic scientists for years is how to accurately identify the time since death, or post-mortem interval. Scientists have been able to estimate time since death based on physical evidence and environmental factors, but it has notoriously proven difficult to quantify this information. It has been difficult for scientists to find a biomarker of post-mortem interval. Herein, we present a Raman study of amino acids to determine possible biomarkers. We also present the first use of spatially offset Raman spectroscopy (SORS) to identify potential biomarkers of post-mortem interval through a whole bovine eye.

Another area where Raman spectroscopy has previously shown to be useful previously is in the study of bone composition. Although the chemical composition of bone is well understood, how bone composition changes through the bone healing process is not as well understood. Here we show the potential

of SORS to be used as a tool to estimate the age of bone fractures by changes in chemical composition over time. It is our hope that in the future this method could be developed further and used to age bone fractures of child abuse victims *in vivo*.

The further development of the results of this work could lead to faster, portable, specific, and nondestructive determination of forensically relevant information from *in vivo* samples. Successful development of these techniques could revolutionize the field of forensic evidence analysis by improving chemical specificity and providing a portable technique with rapid, reliable results.

TABLE OF CONTENTS

LIST OF FIGURES

CHAPTER I.
INTRODUCTION

1.1 Motivation

Raman spectroscopy is a nondestructive, portable technique that utilizes the properties of molecules' interaction with light and the scattering of light by the target molecule to obtain chemical information about a sample. Recently, Raman spectroscopy has become widespread in the areas of forensic science and diagnostics due to its nondestructive and specific nature. Our motivation for using Raman spectroscopy is that the technique gives way to improving the current status of forensic analysis of biological materials. The nondestructive, portable nature of the technique is desirable for use on human subjects because it can be applied non-invasively.

1.2 Raman Spectroscopy

Raman Spectroscopy is a vibrational spectroscopy that involves interaction between a molecule and an electromagnetic field, which leads to vibrational and rotational excitation resulting in the scattering of a photon by a molecule. This effect is known as the Raman Effect, discovered in 1928. The phenomenon of light scattering occurs when there is a collision between a molecule and a photon, resulting in energy being transferred between the two. As shown in Figure 1, after excitation, light can be scattered elastically, resulting in no change in energy (Rayleigh scattering) or inelastically, resulting in a change in energy (Raman scattering).[1] Raman scattering can be classified in one of two ways – Stokes or anti-Stokes. Anti-stokes Raman scattering occurs when an

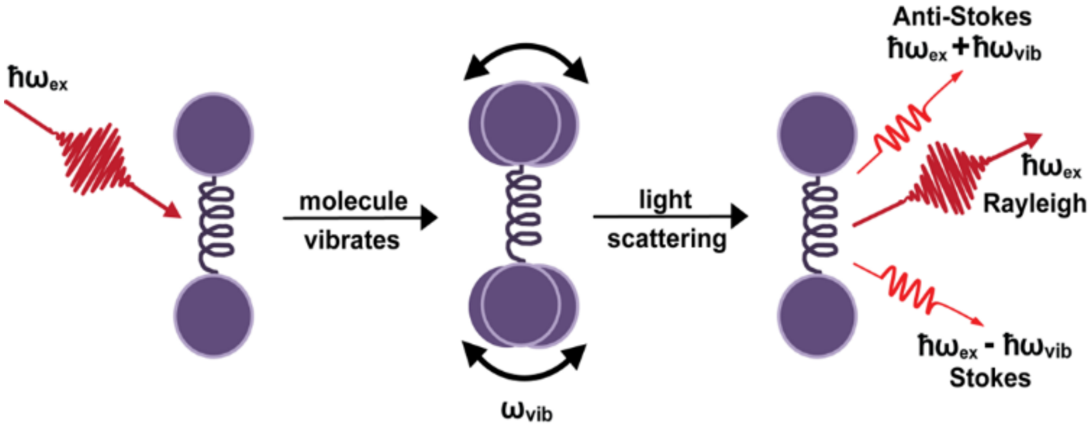

Figure 1. Light Scattering. Interaction of incident light causes a molecule to vibrate and scatter light, either elastically (Anti-Stokes and Stokes) or inelastically (Rayleigh).

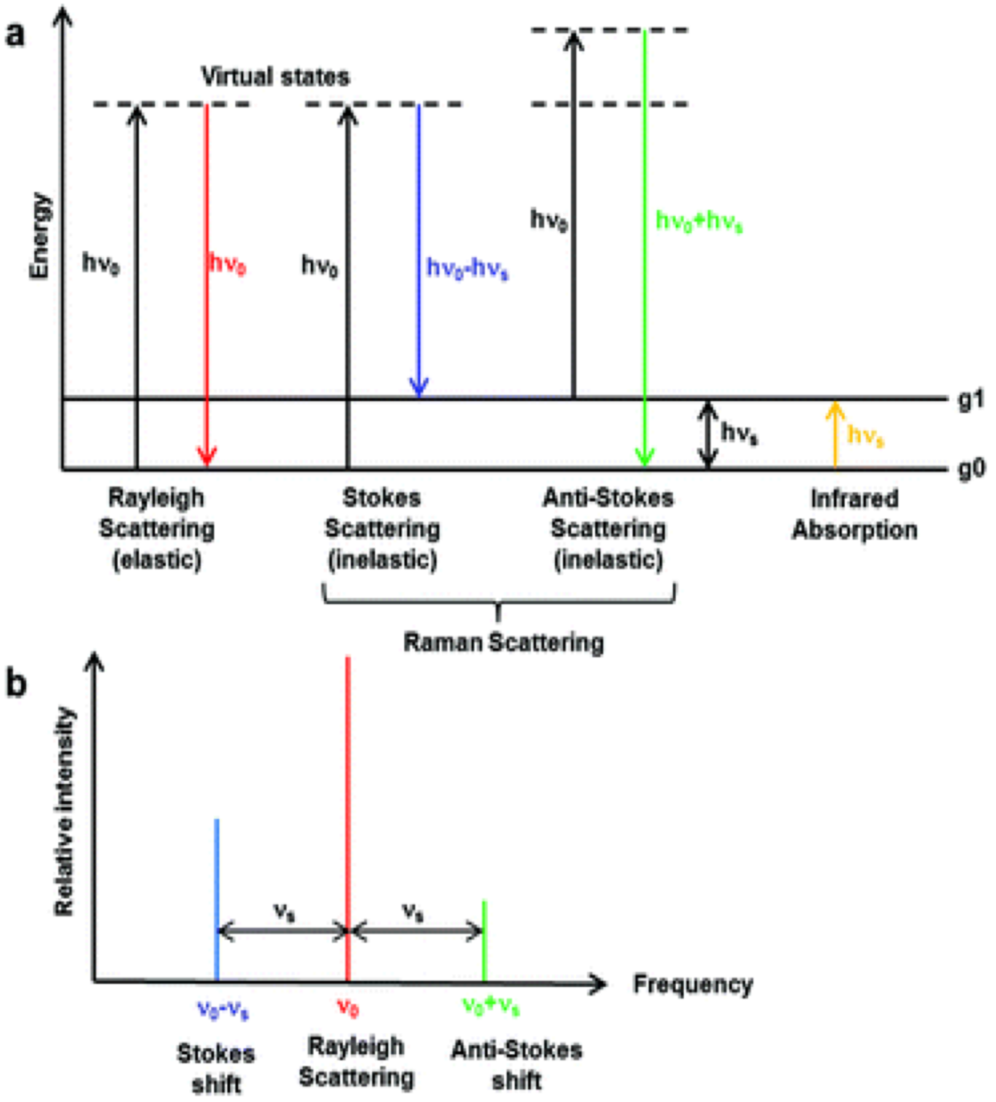

Figure 2. Jablonski Diagram. Reproduced from Lam et. al depicting the energy changes associated with light scattering.[2]

electron in a vibrational level higher than the ground state is excited to a meta-stable transition state, then relaxes down to the ground state. This results in scattered light of a shorter wavelength and higher energy than the incident light. Stokes scattering results in scattered light of a longer wavelength and lower energy than the incident light. As seen in Figure 2a,[2] Stokes scattering occurs when an electron starts in the ground vibrational state, is excited to a metastable virtual state, and relaxes down to a vibrational level higher than the initial energy level. Because electrons are more likely to be found in the ground state due to the ground state being lower in energy and thus more energetically favorable, Stokes scattering is more common. In all the experiments described hereafter, Stokes scattering was utilized.

To be Raman active, a molecule must have a change in polarizability when it vibrates. When monochromatic light is incident on a molecule, the molecule experiences an induced dipole moment given by the equation 1.1, where α is the polarizability, μ is the induced dipole, and E is the electric field.[3]

$$\mu_{\text{induced}} = \alpha * E_{\text{field}} \qquad \text{Equation. 1.1}$$

Raman spectroscopy is a useful technique for several reasons. Raman spectroscopy is chemically specific, meaning it is possible to obtain a unique molecular signature for each chemical component of a sample. It is also a rapid, portable, nondestructive technique that requires little to no sample preparation, which makes this technique appealing to the forensics field.

1.2.1 Spatially Offset Raman Spectroscopy (SORS)

When using conventional Raman spectroscopy, light from a sample is scattered back along the same trajectory as the incident laser light, so the scattering signal measured is from the surface of the sample. Spatially offset Raman Spectroscopy (SORS), allows for deeper levels of a sample to be probed nondestructively than would be possible with conventional Raman. SORS, developed by Matousek et. al,[4] employs the same concepts as conventional Raman, except after the sample is illuminated, spectra are collected at a point offset from the incident light. As the collection point is moved farther from the incident point, the information obtained arises from deeper layers, shown in Figure 3. This is because, due to the photon migration effect, photons migrate laterally through the subsurface layers before scattering back out.[4] As light propagates through the sample, it becomes more evenly dispersed through the subsurface layers, scatters back out, and is collected.

Two main geometries, shown in Figure 4, for collecting signal exist. Signal can be collected in a backscattering (180 degree) geometry, or transmission geometry. Backscattering geometry is more common and involves irradiation of a sample and focusing the collected light back onto the detector. Transmission geometry involves displacing the collection and illumination areas to an extreme extent and is useful in measuring through the bulk of a sample to find an analyte in an unknown location. In our experiments, we will use backscattering geometry because we are targeting specific areas of the samples.

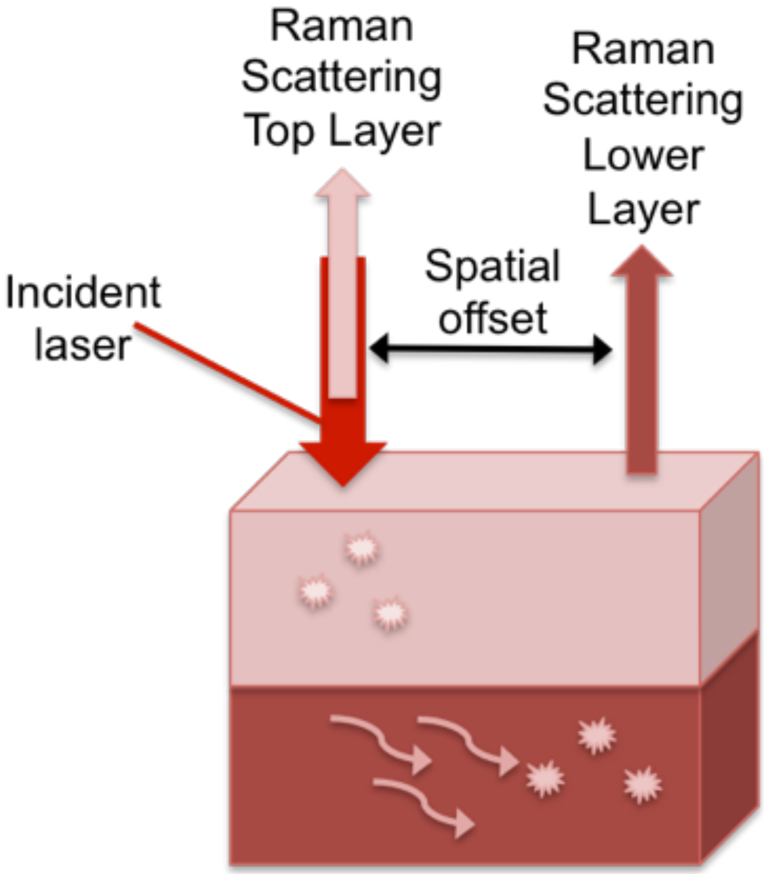

Figure 3. SORS Theory. Incident light enters sample, some light interacts with surface and scatters back out. The rest travels through the sample. Photons migrate laterally and scatter back out, where the scattered light is collected at a spatial offset

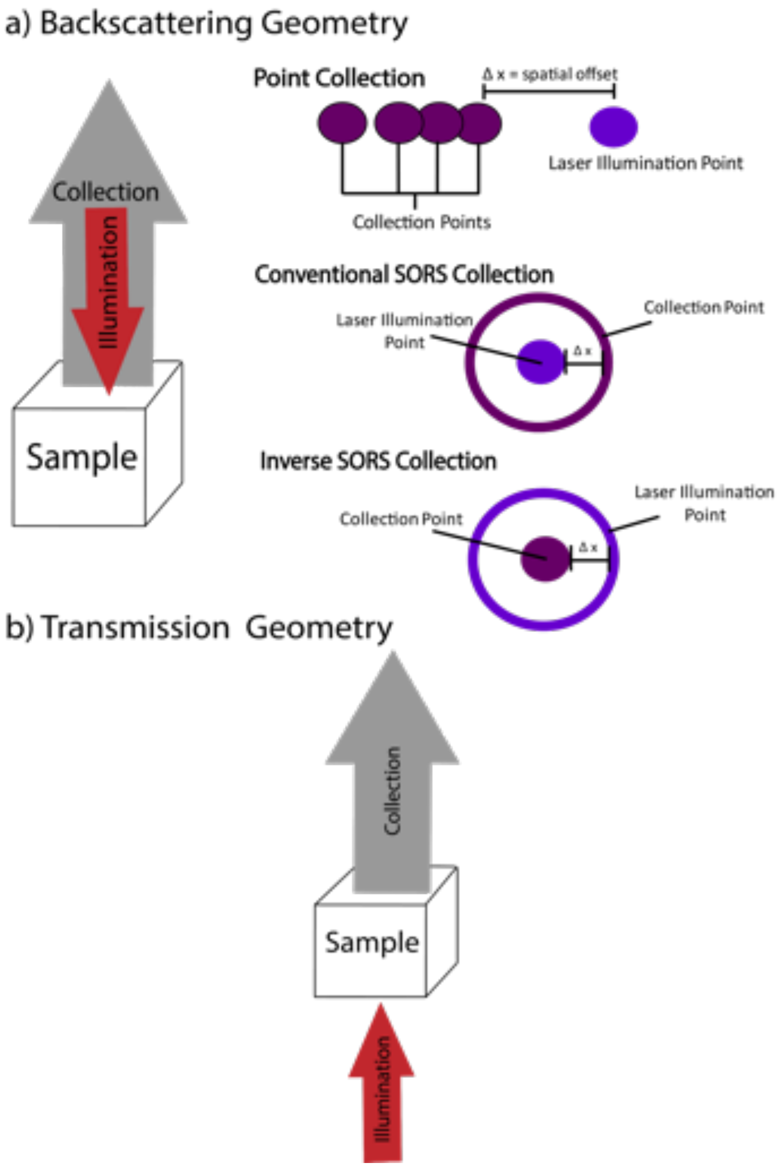

Figure 4. Collection Geometries. There are two types of collection geometries including **a) backscattering** and **b) transmission.** There are three types of backscattering geometry including point collection, conventional SORS collection, and inverse SORS collection.

There are three ways light can be collected in a backscattering geometry, seen in Figure 4. Firstly, point collection involves collecting signal at different zones laterally offset from the point of illumination. This method relies on the user's ability to properly manage optics to achieve the desired offset. Conventional SORS requires illuminating the sample at a point, and signal is collected from a point offset from the illumination, typically by a fiber optic probe. Conventional SORS is limited in what offsets can be achieved because of the diameter of the fiber optic probe, as the fiber optic probe diameter cannot be change. Fiber optic probes increase sensitivity, however, conventional SORS suffers because of spectral distortions caused by different signals being collected at the same time on the CCD camera.[5] The final method to collect SORS signal is called inverse SORS. In this method of signal collection, either a fiber optic probe or a special optical lens called an axicon lens, shown in Figure 5, can be used to create the annular illumination (illumination in a ring).[5,6] An axicon focuses light into beams that form a ring and spatial offset and is simple to manipulate, while also dispersing power over a wider area so that intensity restrictions are yielded.[7] Depth of light propagation can be manipulated easily by moving the axicon so that the ring formed is of the desired offset, where the radius of the ring is the spatial offset and thus the depth propagated. Added benefits of inverse SORS include higher sensitivity, deeper probing depths than conventional SORS, and power is spread over a larger area so larger power can be delivered to tissues *in vivo* without surpassing maximum permissible exposure. In the experiments to be described here, we will be collecting SORS spectra using the inverse SORS collection method using an axicon lens (Figure 5).

1.2.2 Surface Enhanced Raman Spectroscopy (SERS)

The intensity of Raman signal is dependent on the cross-sectional area of the molecule, σ_{RS}, and the photon flux, I_0.[1] This can be described by equation 1.2.

$$I_{RS} = \sigma_{RS}\, I_0 \qquad \text{Equation 1.2}$$

The cross-sectional area of molecules are usually on the order of 10^{-29} cm^2, which can cause Raman intensity to suffer.[8] In the case of weak signal, it is possible to increase signal by using a technique known as surface enhanced Raman spectroscopy (SERS).

SERS utilizes a property of plasmonic metals called the localized surface plasmon resonance (LSPR), shown in Figure 6.[9] Surface conduction electrons of the metal oscillate, creating an enhanced electric field at the junction of the metal nanoparticles, termed a “hot spot”. The LSPR is dependent on size, shape, composition, and dielectric environment.[10] The resulting enhanced electric field along with other factors such as the reduced cross-sectional areas associated with SERS, leads to an increased Raman signal, thus improving signal to noise ratio and sensitivity.[11]

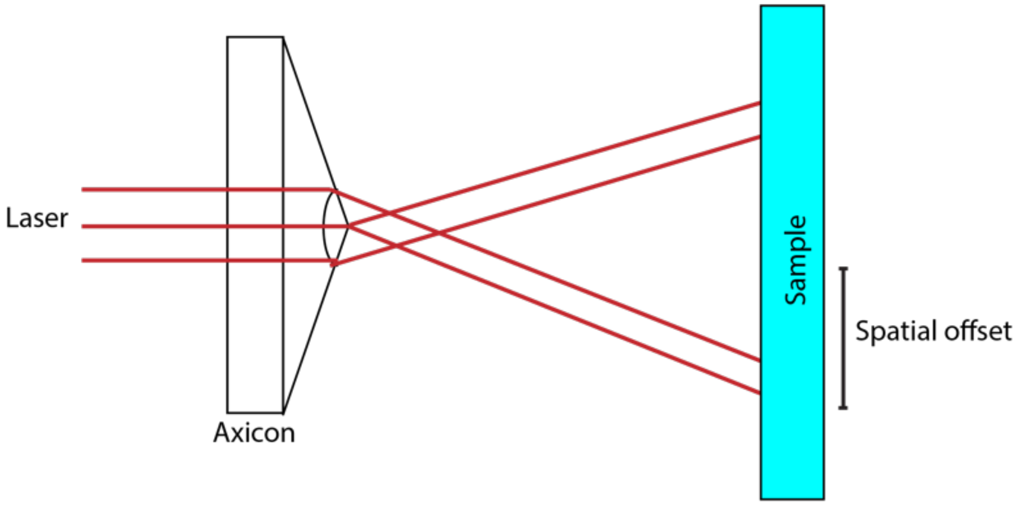

Figure 5.Axicon Lens. Depiction of how an axicon lens directs the beam into a circle. The beam width remains the same around the whole circumference and spatial offset is the radius of the circle.

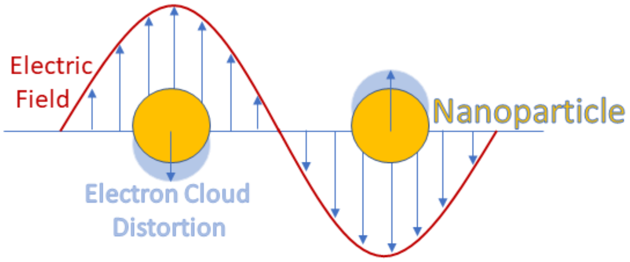

Figure 6. Localized Surface Plasmon Resonance (LSPR). Conduction electrons around on the surface of a metal oscillate and create an increased electric field, enhancing Raman signal.

The capability of nanoparticles to enhance signal can be described by the enhancement factor. This factor is a description of the magnitude of enhancement in SERS signal. Enhancement factor can measure on the order of 10^8.[12] Analytical enhancement factor is described by equation 1.3, where I is intensity, and c is concentration of analyte adsorbed to the nanoparticle surface in the sample.

$$AEF = \frac{I_{SERS}}{I_{RS}} \times \frac{c_{SERS}}{c_{RS}} \qquad \text{Equation 1.3}$$

In these experiments, SERS was combined with SORS, termed SESORS, to determine whether combining SERS with SORS increased the signal in the samples being measured. SERS was also used to look at biomolecules to decide where peaks were that we should expect.

1.3 Instrumentation and Methods

1.3.1 Micro Raman Setup

As shown in Figure 7, a 785 nm diode laser is directed off multiple reflecting mirrors through two irises. Laser light is then directed up into the Ti-U inverted microscope (Nikon) equipped with a 20X magnification objective to the sample. Scattered light from the sample is then sent through a longpass filter, which filters out Rayleigh light. After going through the longpass filter, Raman light enters the spectrometer (Princeton Instruments Isoplane SCT 320) and then is translated into signal on a charge-coupled device (CCD) detector (Princeton Instruments PIXIS 400).

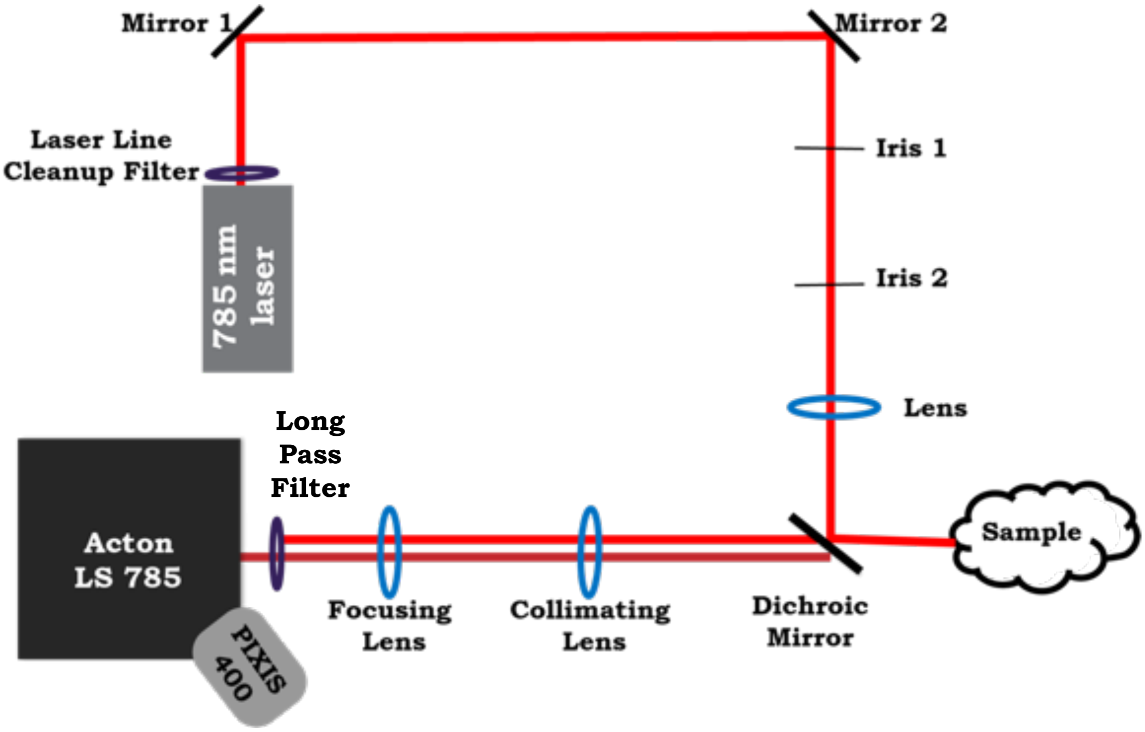

Figure 7. Micro-Raman System. Schematic of homebuilt micro-Raman system equipped with 785 nm laser and CCD camera.

1.3.2 Macro Raman Setup

Shown in Figure 8, a 785 nm diode laser is directed off two mirrors, through two irises, and through a focusing lens, which focuses the laser spot. Light is then directed off a dichroic mirror, which reflects light at a 90° angle onto the sample. Then a lower energy light (Stokes) is scattered back out of the sample at 180 degrees, passes through the other side of the dichroic mirror. The light then goes through a set of collimating lenses, where it is focused onto the spectrometer slit. A holographic longpass filter is then used to filter out Rayleigh light at 785 nm, and the Stokes light enters the spectrometer (Princeton Instruments Acton LS-785), where it is then converted to an image by a CCD detector (Princeton Instruments Pixis 400).

1.3.3 Nanoparticle Synthesis and Characterization

Gold nanoparticles (AuNPs) were synthesized by following a modified Frens synthesis protocol.[13] A 10^{-2} % gold colloid solution was made with 18 MΩ cm ultra-pure water and tetrachloroauric acid ($HAuCl_4$). Next, a 1% citrate solution was made with trisodium citrate ($Na_3C_6H_5O_7$). In an Erlenmeyer flask, 45 mL of gold solution was brought to a boil and 300 μL of citrate solution were added to the boiling solution. The solution should go through color changes until it reaches a dark red/pink color after approximately 5 minutes. At this point, the reaction is complete. Absorption spectra were taken with a UV-Vis Spectrometer (Cary 5000, Agilent) to characterize the nanoparticles. The absorption peak is measured at the wavelength of where the nanoparticles' LSPR occurs, and

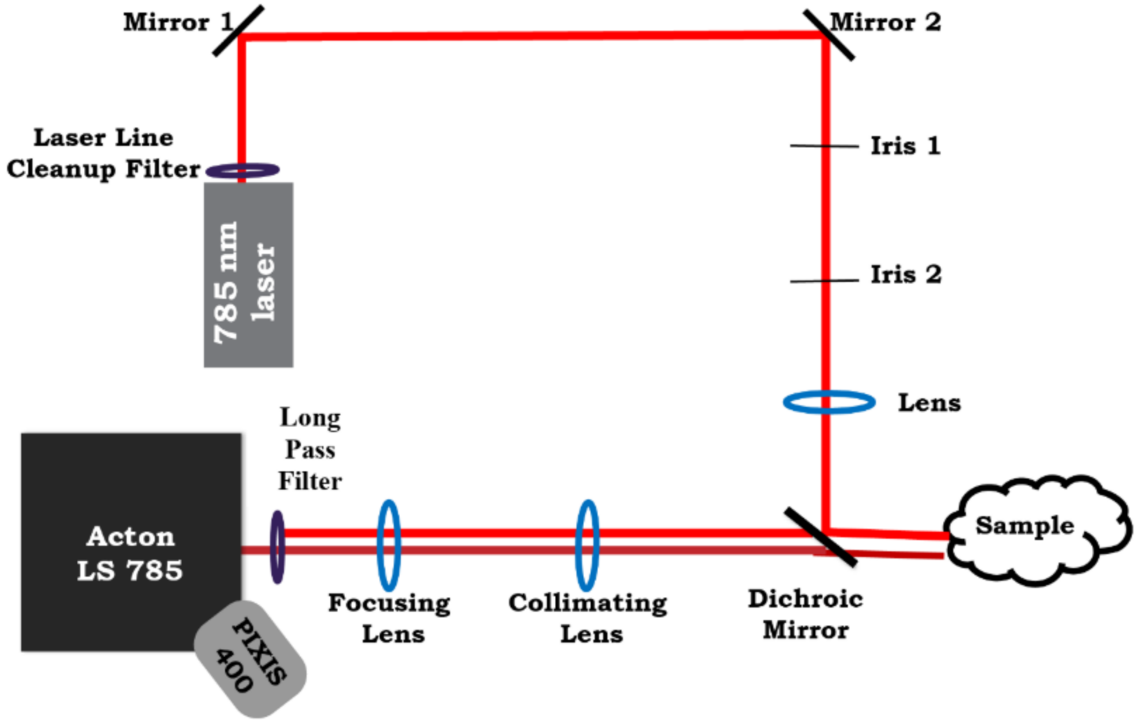

Figure 8. Macro Raman System. Schematic of home-built Raman system in 180 -degree backscattering geometry, equipped with 785 nm laser and a CCD detector.

usually ranges from 525-540 nm for gold. A representative gold absorption spectrum is shown in Figure 9.

Silver nanoparticles (AgNPs) were synthesized by following the Leopold Lendl hydroxylamine method. [14] First, aqua regia was used to clean glassware. A 1 M hydroxylamine hydrochloride solution was made. Then a 1M NaOH solution was made. Next, a 10mM $AgNO_3$ solution was made. Next, 89.995 mL of H_2O, 300 μL of the 1M NaOH, and 150 μL of the hydroxylamine hydrochloride was added to a flask. The solution was stirred on a stir plate at 300 RPM. Lastly, 10 mL of $AgNO_3$ was added all at once and stirred for 5 minutes. Absorption spectra were collected, and the LSPR was typically around 409 nm. To further test nanoparticles, 1 mL of nanoparticle solution was centrifuged. For AuNPs, this was at 4200 RPM for 15 minutes and for AgNPs was at 6000 RPM for 7 minutes. Then supernatant was removed. Next, 200 μL of 100μm benzenethiol (BT) was added to the nanoparticles, which were then diluted to 1 mL with 800μL of 18 MΩ cm ultra-pure water. The solution incubated for 45 minutes, at which point a SERS spectrum was collected, shown in Figure 10. A confocal Raman set-up (20X objective), previously shown in Figure 7 was used. Each SERS spectrum of BT was acquired for 1 s at 5 mW of power at the sample with 785 nm excitation wavelength ($\lambda_{excitation}$) to show that nanoparticles were functionalized and gave appropriate signal. This was completed each time a new batch of nanoparticles was synthesized. Enhancement factors were typically on the order of 10^5.

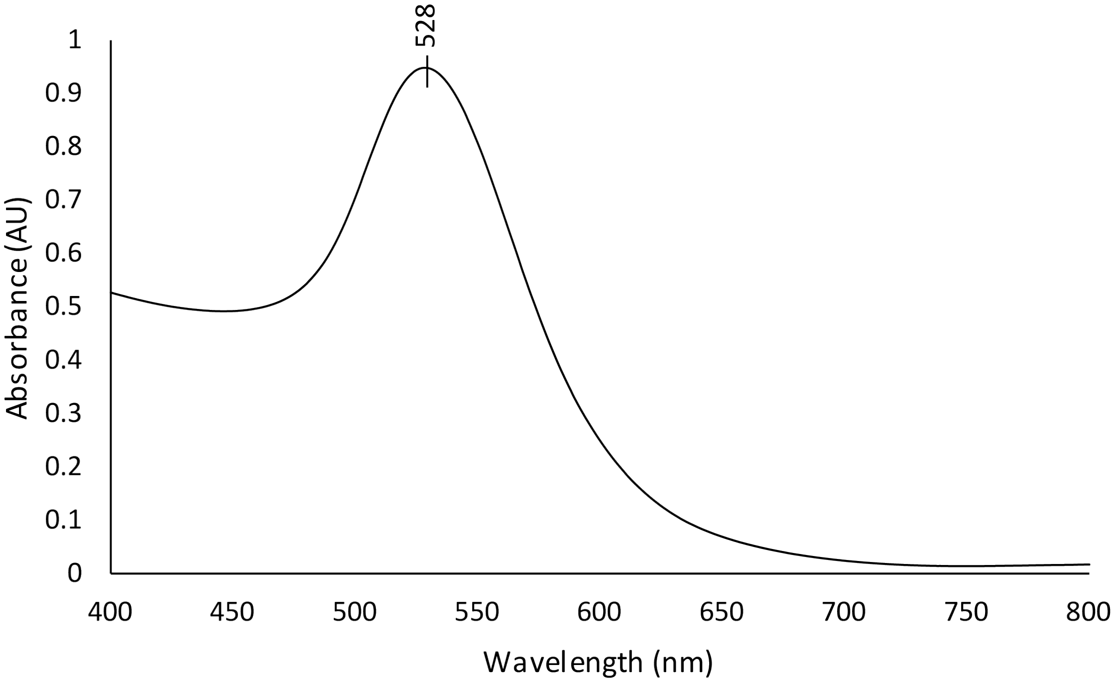

Figure 9. Absorption Spectrum. UV-Vis absorption of gold nanoparticles, showing LSPR at 528 nm.

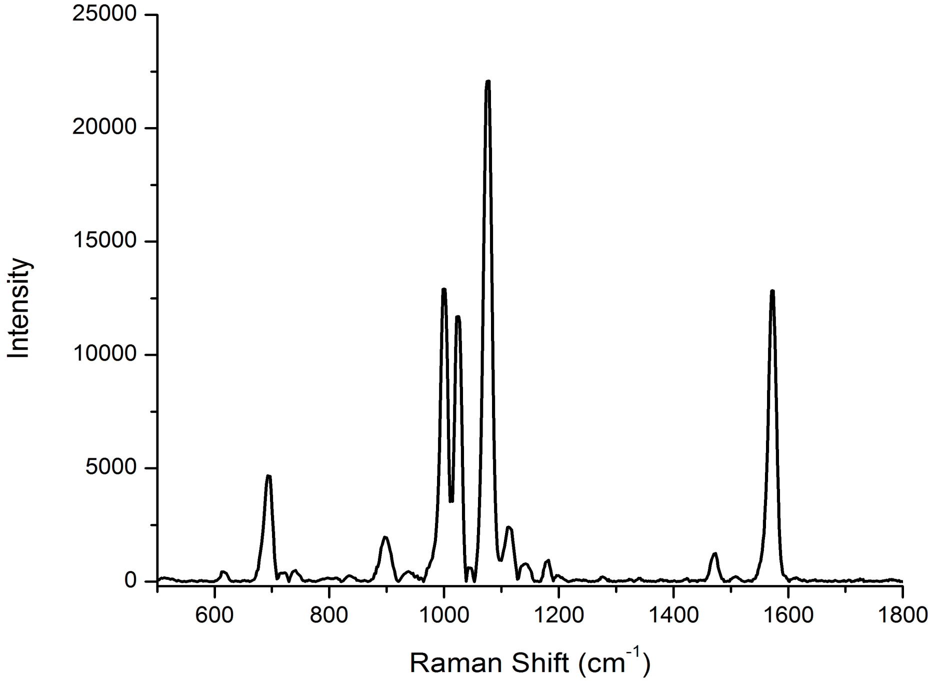

Figure 10. SERS of Benzenethiol. SERS spectrum of benzenethiol on gold nanoparticles, taken at 785 nm, 20X magnification, for 60 s.

1.4 References

1. Corporation, T. E., Introduction to Raman Spectroscopy. In *Molecular Spectroscopy*, 2003.

2. Lam, Z. Y.; Kong, K. V.; Olivo, M.; Leong, W. K., Vibrational spectroscopy of metal carbonyls for bio-imaging and -sensing. *Analyst* **2016,** *141* (5), 1569-1586.

3. Engel, T.; Reid, P.; Engel, T.; Hehre, W., *Physical chemistry*. 3rd ed.; Pearson: Boston, 2013; p xix, 1103 p

4. Matousek, P.; Clark, I. P.; Draper, E. R. C.; Morris, M. D.; Goodship, A. E.; Everall, N.; Towrie, M.; Finney, W. F.; Parker, A. W., Subsurface probing in diffusely scattering media using spatially offset Raman spectroscopy. *Appl Spectrosc* **2005,** *59* (4), 393-400.

5. Matousek, P., Inverse Spatially Offset Raman Spectroscopy for Deep Noninvasive Probing of Turbid Media. *Applied Spectroscopy* 2016, *60* (11), 1341-1347.

6. Matousek, P.; Clark, I. P.; Draper, E. R. C.; Morris, M. D.; Goodship, A. E.; Everall, N.; Towrie, M.; Finney, W. F.; Parker, A. W., Subsurface Probing in Diffusely Scattering Media Using Spatially Offset Raman Spectroscopy. *Applied Spectroscopy* **2016,** *59* (4), 393-400.

7. Matousek, P.; Stone, N., Development of deep subsurface Raman spectroscopy for medical diagnosis and disease monitoring. *Chemical Society Reviews* **2016,** *45* (7), 1794-1802.

8. Aroca, R., *Surface-Enhanced Vibrational Spectroscopy*. John Wiley & Sons, Ltd.: England, 2006.

9. King, F. W.; Van Duyne, R. P.; Schatz, G. C., Theory of Raman scattering by molecules adsorbed on electrode surfaces. *The Journal of Chemical Physics* **1978,** *69* (10), 4472-4481.

10. Stiles, P. L.; Dieringer, J. A.; Shah, N. C.; Van Duyne, R. R., Surface-Enhanced Raman Spectroscopy. *Annual Review of Analytical Chemistry* **2008,** *1*, 601-626.

11. Sharma, B.; Fernanda Cardinal, M.; Kleinman, S. L.; Greeneltch, N. G.; Frontiera, R. R.; Blaber, M. G.; Schatz, G. C.; Van Duyne, R. P., High-performance SERS substrates: Advances and challenges. *MRS Bulletin* **2013,** *38* (08), 615-624.

12. Greeneltch, N. G.; Blaber, M. G.; Schatz, G. C.; Van Duyne, R. P., Plasmon-Sampled Surface-Enhanced Raman Excitation Spectroscopy on Silver Immobilized Nanorod Assemblies and Optimization for Near Infrared (lambda(ex)=1064 nm) Studies. *Journal of Physical Chemistry C* **2013,** *117* (6), 2554-2558.

13. Frens, G., Controlled Nucleation for the Regulation of the Particle Size in Monodisperse Gold Suspensions. *Nature Physical Science* **1973,** *241*, 20-22.

14. Leopold, N.; Lendl, B., A New Method for Fast Preparation of Highly Surface-Enhanced Raman Scattering (SERS) Active Silver Colloids at Room Temperature by Reduction of Silver Nitrate with Hydroxylamine Hydrochloride. *The Journal of Physical Chemistry B* **2003,** *107* (24), 5723-5727.

CHAPTER II

RAMAN AND SURFACE ENHANCED RAMAN SIGNATURES OF POTENTIAL BIOMARKERS

This chapter details the collection of normal Raman and SERS signatures of potential biomarkers that had been determined by previous studies in the literature to be of particular interest as biomarkers in determining post-mortem interval. [3],[4-12] Uric acid, lactic acid, hypoxanthine, phenylalanine, tyrosine, tryptophan, L-proline, L-alanine, and L-glycine were studied by various methods detailed here.

2.1 Abstract

The presentation of scientific evidence in criminal cases is of paramount importance, oftentimes being the deciding factor in if a person is declared innocent or guilty. For this reason, forensic testing methods need to be as accurate and specific as possible. One of the most important pieces of a case is the estimated time of death, otherwise known as the post-mortem interval (PMI). Historically, physical changes such as rigor mortis, have been used to determine the PMI. Studies of temperature cooling, gastric contents, putrefaction, and entomology have also been used. Although these methods provide a general estimate, it would be desirable to determine a more specific window for time of death. Raman spectroscopy and surface enhanced Raman spectroscopy could be utilized to nondestructively and quickly determine time since death by estimating a more specific time frame of PMI. The first step in using this technique to estimate PMI is to determine which biomarkers should be targeted. We chose to investigate biomarkers previously mentioned in literature using normal Raman and SERS with both gold and silver nanoparticles to determine what molecules we should target.

2.2 Introduction

Forensic scientists face numerous challenges in their day to day work. One of the most important yet difficult pieces of information to determine in a death investigation is the time elapsed since death, also known as the post-mortem interval, or PMI.

Death is scientifically defined as when respiratory, brain, and circulatory function cease irreversibly. [1] Several changes occur post-mortem, including supravitality, livor mortis, and rigor mortis. Supravitality refers to when an organism's tissues can still metabolize, but the organism is dead. Metabolism in the early stages after death occurs by anaerobic glycolysis and the creatine kinase reaction. Information learned from early post-mortem stages could be used to estimate PMI. [1] Livor mortis, rigor mortis, and algor mortis have been signals for estimating PMI since the 1800s. [2] Livor mortis is the first stage after death, and it is characterized by pooling of blood at the bottom of a corpse. In the beginning of livor mortis, blood is light pink colored, but it can turn dark colored due to the lack of oxygen as time goes on. [1] Rigor mortis develops starting at 3-4 hours after death, starts in the face, and proceeds to larger muscles, including skeletal and smooth muscles, and lasts up to 76 hours. After death, muscles become flaccid, but during rigor mortis, the creatine kinase reaction produces ATP by anaerobic glycolysis. As this happens, actin and myosin in muscle still form bridges, and this allows the muscle to still contract after death. Muscles can stay rigid, in their contracted state, up to 76 hours. The end of rigor mortis is signaled by the increase in concentration of ammonia, indicating protein degradation. [1] The time and extent of rigor mortis is highly variable and can be influenced by many factors such as temperature, environmental factors, and the amount of glycogen in the muscles at the time of death. Algor mortis refers to the cooling of the body after death and occurs in three stages: the initial phase, the intermediate stage, and the terminal phase. During the initial phase, which occurs right after death, the body temperature remains constant. When the body temperature decreases rapidly, the intermediate phase of algor mortis occurs. The terminal phase is when the body cools down to the temperature of its surroundings. [1]

Complications in estimating PMI are introduced when PMI estimation is based solely on observation because of variability in the environment and circumstances surrounding the death. There is a need to determine PMI more quantitatively to increase accuracy. Previous studies have identified possible biomarkers of post-mortem interval including hypoxanthine, uric acid, formate, lactate, amino acids, and acetate, among others. [3,4-12] Hypoxanthine is a product of purine degradation, which has been identified in multiple studies as a potential biomarker for PMI. [3, 5-6, 9] Since proteins degrade with time, it is proposed that increase in amino acid concentration might also be indicative of post-mortem interval. Appanna, Donaldson and Lamont aimed to investigate pH changes and concentration changes of six metabolites, including lactic acid, hypoxanthine, ammonia, NADH, and formic acid post-mortem from blood samples using assays. [5] They determined that hypoxanthine, ammonia, and NADH could be the best indicators of PMI in blood. Another study by Kage et al. determined concentrations of formate and acetate simultaneously in post-mortem blood by GC-MS. [7]

It is necessary to determine what tissue is most suitable for PMI estimation. For this reason, Zelentsova et al. used HPLC and NMR to study changes in 61 different metabolites in post-mortem rabbit blood serum and ocular fluids in order to determine which fluid was more suited for PMI estimation. [3] Serum and ocular fluids were collected before death and at intervals of 1, 2, 4, 6, 10, 14, 23, and 31 hours post-mortem and metabolites were quantified. It was determined that hypoxanthine, choline, and glycerol showed the most significant and linear increase in concentration with time and metabolic changes happen much slower in aqueous humor (AH) and vitreous humor (VH) samples than in blood. Ocular fluids also showed less data scattering, indicating that AH and VH samples are better suited for PMI analysis than blood samples.

Investigations into biomarkers of PMI and indicators of disease in aqueous and vitreous humors have been attempted, but these studies have used invasive, destructive, less specific, and/or time consuming methods like GC, LC-MS, UV-Vis, ion-selective electrodes, and photometry. [9, 11] Thierauf et al. used photometric methods and electrochemistry and showed that sodium, potassium, calcium, chloride, urea, creatinine, glucose, and lactate could be observed in vitreous humor. [11] Patrick and Logan have observed amino acids in vitreous by an amino acid analyzer after much sample preparation; they determined that amino acid concentrations were directly related to post-mortem interval, and taurine, glycine, alanine, phenylalanine, and histidine contributed the most to vitreous total amino acid content. [13] Ansari et al. used silver nanoparticle (AgNP) based sensors with colorimetric detection to study cysteine as a potential marker of time since death, and they determined a limit of detection of 0.007 µg/mL for cysteine in vitreous, as well as a linear correlation with increasing PMI. [4] Girela et al. studied amino acid concentrations in vitreous humor and cerebrospinal fluid (CSF) using HPLC. [14] They determined taurine, glutamate, and aspartate, which are all amino acids, increased in concentration with statistical significance in vitreous humor as PMI increased. Snytnikova et al. looked at the metabolomics of the human cornea and aqueous humor using NMR and HPLC with high resolution ESI-MS detection. [15] They found that concentrations of purines and organic acids in the cornea are higher than in the aqueous humor, indicating the cornea could be a better target than the aqueous humor. Based on these studies, amino acids, urea, creatinine, glucose, and lactate in vitreous or compounds in the cornea could be possible targets for the use of Raman spectroscopy to determine PMI. [4, 11, 13-15]

We aimed to determine which biomarkers suggested should be targeted in future studies. We utilized various methods of normal Raman and SERS nanoparticles to study which biomarker would be an ideal target for studying time of death in eye tissue. Here we studied uric acid, lactic acid, phenylalanine, tyrosine, tryptophan, L-proline, L-alanine, adenine, L-glycine, and hypoxanthine.

2.3 Methods

Raman spectra of solid uric acid, lactic acid, and hypoxanthine were each collected at 5 mW of power for 60 seconds with a 785 nm excitation wavelength. Next, 100 mM solutions were made of each and normal Raman spectra were collected with the same parameters. Samples were then diluted to their desired concentrations which were based on their solubility limits. For each separate sample, 1 mL of AuNPs were centrifuged at 4200 RPM for 15 minutes. Then, 100 µL of each sample solution were added to the AuNPs and incubated for 45 minutes. Hydroxylamine silver nanoparticles were also used to detect these molecules following the same procedure, apart from changing time and speed centrifuged to 7 minutes at 6000 RPM. Raman spectra of these solutions were collected at 785 nm excitation at 5mW of power and 60 s acquisition time.

Proteins are of abundance in the human body, especially in the eye lens, so we were also interested in studying the optimal way to detect amino acids using SERS. Amino acids tyrosine, tryptophan, phenylalanine, L-alanine, L-proline, and glycine were studied using SERS on both the micro and macro systems. SERS gold nanoparticle (AuNP) samples were prepared by spinning down 1mL of AuNPs in a centrifuge at 4200 RPM for 15 minutes. Hydroxylamine silver particles (AgNPs) were prepared by spinning 1mL in the centrifuge for 7 minutes at 6000 RPM. Then, 200 µL of the specified sample were added to the respective particles. SERS spectra collected on the micro- system were collected at 785 nm excitation wavelength, 5 mW of power, 20X objective, and 60 s acquisition time. SERS spectra collected on the macro system were collected at 785 nm excitation wavelength, 90 mW of power, and 60 s acquisition time. Normal Raman spectra collected were from the solid sample and the 100mM sample, both being collected at 90mW of power and 785 nm excitation wavelength on the macro-system and 5 mW of power and 785 nm excitation on the micro-system. SERS spectra were collected from solutions ranging in concentration from 100 µM to 100 mM. pH of each sample was also adjusted when necessary by adding 1 µL of 3M HCl before spectra collection.

2.4 Results and Discussion

It was determined that gold nanoparticles should be used when analyzing lactic acid, uric acid, and hypoxanthine because they resulted in increased signal. Limits of detection (LOD) and optimum pH were also studied. Eventually, it was decided to not move forward with these studies on lactic acid, uric acid, and hypoxanthine, however, as we were concurrently studying biological materials and were not seeing these molecules within the materials we were interested in. Although the information gained from these analytes was not useful for our purposes and thus not shown here, we were able to show that lactic acid, uric acid, and hypoxanthine can be detected using SERS if need be.

As seen in Figure 11, it was shown that phenylalanine, tryptophan, and tyrosine SERS spectra were easily measured on the micro-system with AuNPs. Their spectra are shown here. The other analytes did not have as good of SERS spectra on the micro-system and are not shown here. It was determined that the three analytes most suited to measuring on the micro-system with AuNPs were tryptophan, tyrosine, and phenylalanine. It can be seen in Figure 11 that each of these three analytes showed distinct Raman spectra with multiple peaks only appearing in the molecule of interest. This indicated that if we were to measure SERS spectra of these three analytes, it would be desirable to use gold nanoparticles at 785 nm excitation.

The amino acids most suited to SERS measurement on the macro-system with hydroxylamine AgNPs were phenylalanine, proline, and alanine. As seen in Figure 12, Raman signal of these three analytes showed prominent peaks that were not attributed to the hydroxylamine nanoparticles. The other analytes had resulted in spectra that were mostly contributed to by the nanoparticles, so it was determined that this was not the optimum method for tryptophan or tyrosine.

2.5 Conclusions and Future Work

It was concluded that SERS spectra of amino acids of interest in biological applications could be collected on both the micro- and macro-Raman systems in the Sharma lab. The best SERS signal was obtained from phenylalanine on both systems as well as with both types of nanoparticles. Phenylalanine SERS spectra could be measured in various ways, it was determined that phenylalanine is most likely the best target analyte for our studies into post-mortem interval, as it gives a strong Raman signal.

a) Phenylalanine and AuNPS

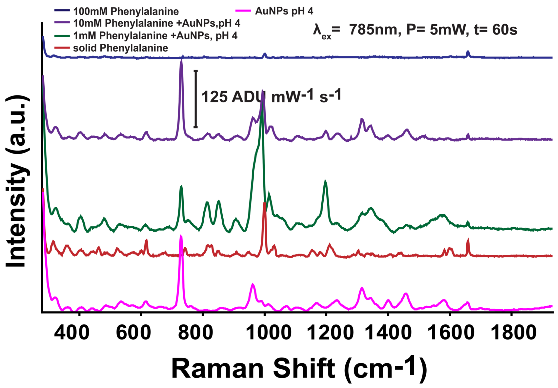

b) Tryptophan and AuNPs

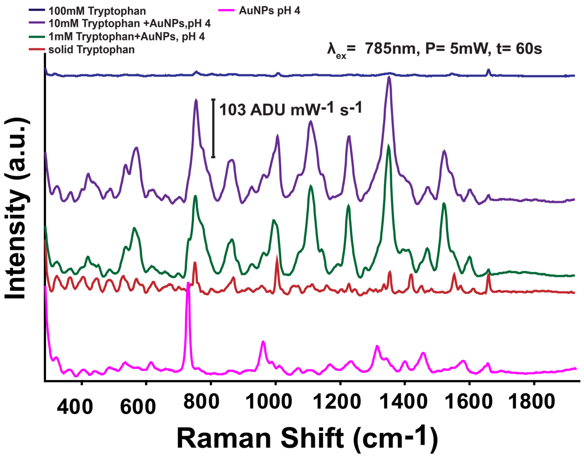

c) Tyrosine and AuNPs

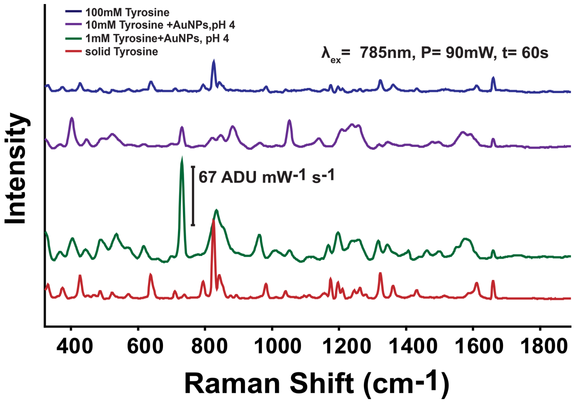

Figure 11. SERS of Amino Acids with gold nanoparticles. The amino acids a) phenylalanine, b) tryptophan, and c) tyrosine gave the best Raman signal out of the amino acids tested with gold on the micro-system. Spectra were collected on the micro system at 785 nm excitation, 5mW of power, and 60 second acquisition time.

a) Phenylalanine and AgNPs

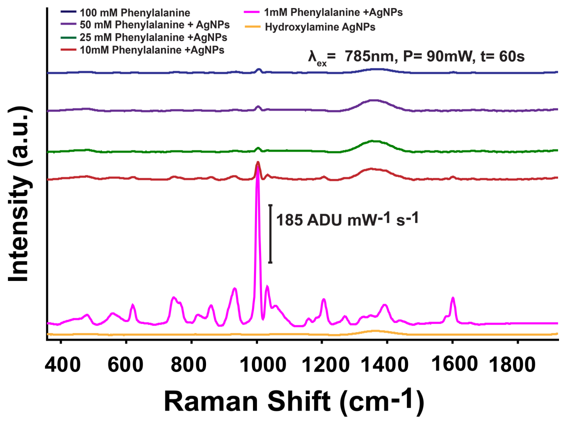

b) Alanine and AgNPs

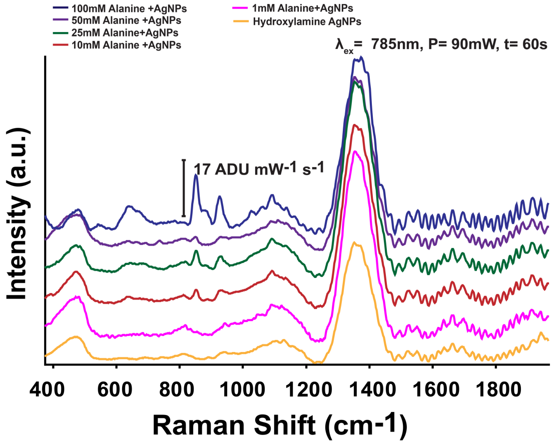

c) Proline and AgNPS

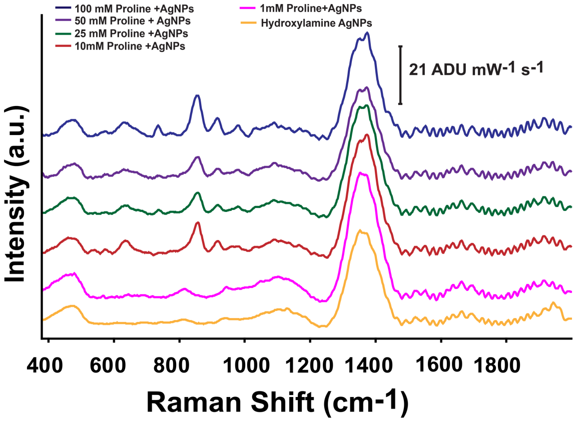

Figure 12. SERS of Amino Acids with hydroxylamine silver nanoparticles. The amino acids phenylalanine, alanine, and proline gave the most distinct SERS spectra on the macro- Raman setup with AgNPs at 785 nm excitation, 90mW of power, and 60 s acquisition time.

For our purposes, we were solely interested in whether or not we could measure the signal of these amino acids and what kind of particles we would need to use to detect them, so more investigation in regards to the specific parameters that should be used to detect these amino acids remains. Future work would be to optimize conditions used to measure SERS spectra of amino acids. We would need to test different incubation times, different pH values, as well as different power directed onto the samples. We could also try to use different shapes and sizes of nanoparticles to enhance detection. Micro-flowers, nanorods, or nanostars could further increase the signal obtained from amino acids and may make the amino acids that were hard to detect more detectable. Once we obtain optimum signal, it would be necessary to determine the limits of detection for each amino acid.

2.6 References

1. Madea, B.; Kernbach-Wighton, G., Early and Late Postmortem Changes. In *Encyclopedia of Forensic Sciences*, 2013; pp 217-228.

2. Madea, B., Estimation of the Time Since Death. In *Encyclopedia of Forensic Sciences*, 2013; pp 229-238.

3. Zelentsova, E. A.; Yanshole, L. V.; Snytnikova, O. A.; Yanshole, V. V.; Tsentalovich, Y. P.; Sagdeev, R. Z., Post-mortem changes in the metabolomic compositions of rabbit blood, aqueous and vitreous humors. *Metabolomics* **2016,** *12* (11).

4. Ansari, N.; Lodha, A.; Menon, S. K., Smart platform for the time since death determination from vitreous humor cystine. *Biosensors and Bioelectronics* **2016,** *86*, 115-121.

5. Appanna, Vasu D.; Donaldson, A. E.; Lamont, I. L., Biochemistry Changes That Occur after Death: Potential Markers for Determining Post-Mortem Interval. *PLoS ONE* **2013,** *8* (11).

6. Donaldson, A. E.; Lamont, I. L., Estimation of post-mortem interval using biochemical markers. *Australian Journal of Forensic Sciences* **2013,** *46* (1), 8-26.

7. Kage, S.; Kudo, K.; Ikeda, H.; Ikeda, N., Simultaneous determination of formate and acetate in whole blood and urine from humans using gas chromatography–mass spectrometry. *Journal of Chromatography B* **2004,** *805* (1), 113-117.

8. Keltanen, T.; Nenonen, T.; Ketola, R. A.; Ojanperä, I.; Sajantila, A.; Lindroos, K., Post-mortem analysis of lactate concentration in diabetics and metformin poisonings. *International Journal of Legal Medicine* **2015,** *129* (6), 1225-1231.

9. Munoz, J. I.; Costas, E.; Rodriguez-Calvo, M. S.; Suarez-Penaranda, J. M.; Lopez-Rivadulla, M.; Concheiro, L., A high-performance liquid chromatography method for hypoxanthine determination in vitreous humour: application to estimation of post mortem interval. *Hum Exp Toxicol* **2006,** *25* (5), 279-81.

10. Pittner, S.; Ehrenfellner, B.; Zissler, A.; Racher, V.; Trutschnig, W.; Bathke, A. C.; Sänger, A. M.; Stoiber, W.; Steinbacher, P.; Monticelli, F. C., First application of a protein-based approach for time since death estimation. *International Journal of Legal Medicine* **2016,** *131* (2), 479-483.

11. Thierauf, A.; Musshoff, F.; Madea, B., Post-mortem biochemical investigations of vitreous humor. *Forensic Science International* **2009,** *192* (1-3), 78-82.

12. Vass, A. A.; Barshick, S. A.; Sega, G.; Caton, J.; Skeen, J. T.; Love, J. C.; Synstelien, J. A., Decomposition chemistry of human remains: a new methodology for determining the postmortem interval. *J Forensic Sci* **2002,** *47* (3), 542-53.

13. Patrick, W. J.; Logan, R. W., Free amino acid content of the vitreous humour in cot deaths. *Archives of Disease in Childhood* **1988,** *63* (6), 660-662.

14. Girela, E.; Villanueva, E.; Irigoyen, P.; Girela, V.; Hernández-Cueto, C.; Peinado, J. M., Free Amino Acid Concentrations in Vitreous Humor and Cerebrospinal Fluid in Relation to the Cause of Death and Postmortem Interval. *Journal of Forensic Sciences* **2008,** *53* (3), 730-733.

15. Snytnikova, O. A.; Yanshole, L. V.; Iskakov, I. A.; Yanshole, V. V.; Chernykh, V. V.; Stepakov, D. A.; Novoselov, V. P.; Tsentalovich, Y. P., Quantitative metabolomic analysis of the human cornea and aqueous humor. *Metabolomics* **2017,** *13* (12).

CHAPTER III
SORS OF THE EYE FOR POST-MORTEM INTERVAL DETERMINATION

This chapter details the use of SORS to measure through different areas of bovine eyes for the potential to determine post-mortem interval. SORS spectra at 3 different spatial offsets (0,2, and 5mm) were collected through the front, side, and back of bovine eyes. Results showed that measuring through the front of the eye is promising for detecting biomarkers, and measuring through the side and back of the eye resulted in collagen signatures. This is the first that we know of that SORS has been used to measure through the whole eye.

A version of this chapter is being prepared for submission to The Journal of Raman Spectroscopy in Summer 2020.

3.1 Abstract

Composition of the eye has been studied for years because of the prevalence of eye disease. It has also recently been suggested that the eye could contain biomarkers that are indicative of post-mortem interval (the time passed since death). Studying the composition of the eye could lead to improved medical and forensic methods. Previous studies have utilized methods such as GC-MS, LC-MS, UV-Vis, and photometry. However, these methods are often destructive and invasive. It is desirable to use a nondestructive, fast, specific, and portable technique to observe the chemical composition of the eye. This is the first study to date to our knowledge that has used spatially offset Raman Spectroscopy (SORS) to study the eye. SORS was used to probe through the front, side, and back of whole bovine eyes at different depths *ex vivo*. Raman signatures arising from the crystalline proteins of the lens can be observed through the front of the eye, and collagen can be observed through the side and back of the eye. It was concluded that SORS can detect biomolecules non-destructively below the surface of the eye and could be useful to diagnose disease or determine post-mortem interval using biomarkers of the eye in the future.

3.2 Introduction

Understanding the composition of the eye could be useful in understanding diseases that affect millions of people worldwide. According to the

National Eye Institute, by 2030, 3.7 million Americans will have age-related macular degeneration, 4.3 million will have glaucoma, 11.3 million will have diabetic retinopathy, and 38.7 million will have cataract disease. [1] These numbers will increase as time goes on, making it imperative to diagnose these diseases early on. The eye is not only of interest in the study of disease, but it also serves as an accessible point for biomarker testing. It has been suggested that biomarkers in various parts of the eye such as amino acids could be useful to the forensics field for post-mortem interval determination. [2-3]

Numerous methods including GC-MS, LC-MS, UV-Vis, and photometry have been used to measure biomarkers in the eye, but these methods are commonly invasive, destructive, less specific, and/or tedious. [4-5] Raman spectroscopy is a nondestructive, noninvasive method that has previously been used to study eye components. In 1975, Yu et al. [6] used Raman spectroscopy to study the water soluble proteins of bovine lens and determined that they contained mostly antiparallel pleated sheet structure in main chains and sulfhydryl groups are localized in g-crystallin proteins. In 1982, Yu et al. showed that it was possible take Raman spectra of a live rabbit lens in situ. [7] Bot et al. used Raman spectroscopy to study intact fresh and paraformaldehyde fixed rabbit lens slices. [8] In the same study, they compared the Raman spectrum of a human lens with the Raman spectrum of a slice of the same human lens. It was concluded that paraformaldehyde had little effect on the lens spectrum and that the Raman spectra of whole lenses and lens slices were comparable; they also concluded that lens slices could be used to lessen fluorescence and improve accuracy of position at which Raman spectra are recorded. In 1991, Sokolov et al. used surface enhanced Raman spectroscopy (SERS) to look at eye lens extracts, and they concluded that SERS is effective in probing biomolecules in human and chipmunk lenses. [9] They determined that adenosine-containing molecules were abundant, and tyrosine and tryptophan signals were intense in cataract samples from humans. Vrensen et al. studied protein profiles in the superficial cortex, deep cortex, and nucleus of aged human lenses using micro-Raman spectroscopy, and found that there was no significant difference in protein profiles in the three different regions. [10] They also were able to give peak assignments to the Raman spectra of the lenses. Glutamate has also been identified in the eye by Raman spectroscopy. [11] A study by Prieto-Bonete et al. showed that morphological and histological changes in the eye lens could be useful for estimating post-mortem interval. [12] Although previous research has provided useful information about the chemical composition of the eye, no method that we are aware of has been used to probe multiple layers of an eye without destroying the eye, which is why we aimed to apply spatially offset Raman spectroscopy (SORS) to measure through multiple layers of the eye.

Spatially offset Raman spectroscopy is a variant of Raman that is useful to probe multiple layers of a sample. When using conventional Raman, light is scattered back at the same point as the sample was illuminated, so most of the signal is from the surface. By using spatially offset Raman spectroscopy (SORS), deeper levels of a sample than would be possible using conventional Raman can be probed nondestructively. SORS, discovered by Matousek et al., employs the same concepts as normal Raman, except after the sample is illuminated, spectra are collected at a point offset from the incident light. [13] As the collection point is moved farther from the incident point, the information obtained comes from deeper layers. With increased offset from the incident point, the top layer contribution is lessened, and contribution from deeper layers is seen. This is because of the migration of photons in the subsurface layers before light is scattered back out, referred to as the photon migration effect. [13] As light travels through the sample, it becomes more evenly dispersed through the subsurface layers then it scatters back out, and signal is collected at an offset. When using an offset, the spectrum contains more chemical information from subsurface layers than from the zero-point offset.

As previously stated in Chapter 1, the two types of SORS collection include point collection and inverse (concentric circle) collection.[14-15] Concentric circle collection is easier to do manually and also gives higher collection efficiency.[15] To achieve an offset, an optical lens called an axicon is used. An axicon works by focusing the light into beams that cross the optical axis and form a ring. The offset is the radius of the ring, which can be manipulated by varying the distance of the axicon from the sample Although the diameter of the ring is varied to obtain different offsets, the width of the ring itself is maintained.

Utilizing concentric circle collection SORS will allow for rapid, non-invasive detection of biomarkers in the eye. Probing the eye non-invasively (i.e. without requiring cutting into the eye) will allow for a potential for easier, safer, faster diagnosis of diseases such as glaucoma, macular degeneration, blindness, etc., as well as provide a method to measure biomarkers of post-mortem interval for forensic purposes. Here we present the first instance that we know of showing that SORS can be used to ascertain chemical information from different layers in multiple locations of the eye.

3.3 Methods

Fresh bovine eyes (n=2) were purchased from Nebraska Scientific. Eyes were immediately subjected to testing upon arrival after being stored on dry ice through transit. After removal of excess tissue, each of the whole eyes was subject to spatially offset Raman spectroscopy (SORS). A home-built macro-Raman system with 180-degree backscattering geometry and was used. The system was equipped with a 785-nm diode laser, spectrometer (Princeton Instruments Acton LS-785), and CCD camera (Princeton Instruments Pixis 400). Concentric circle collection was used, with spatial offset created by an axicon lens. SORS spectra were measured using 0mm, 2mm, and 5 mm spatial offsets through the front, side, and back of each whole eye in order to measure through different layers of the eye. Spectra were collected at 25mW of illumination power in three 60s frames, totaling 3 minutes of collection time at each spot. After spectra were collected from whole eyes, the eyes were dissected, and lenses were isolated. Raman spectra of each lens were taken (785nm, 25mW, 60s, 3 frames). Data collected was averaged using home-written Matlab code and subsequent average spectra were baselined and processed with Grams/AI software.

3.4 Results and Discussion

Averaged spectra show that through the back of the eyes (Figure 13a and d) and the side of the eyes (Figure 13b and e), the peak around 939 cm^{-1} was found in all three spectra for both eyes. This peak is attributed to the C-C stretch of the collagen backbone.The vitreous humor, located in the posterior of the eye, is known to be comprised mainly of collagen, and this is supported by the observation of the 939 cm^{-1} collagen peak in these spectra. It is seen in these spectra that noise is drastically decreased through the 5mm offset, indicating a 5mm offset would be optimal to minimize noise when measuring posterior components of the eye. It is thought that the noise from the 0 and 2mm offset spectra arises from the fluorescent nature of the sclera. Measuring through 5mm completely passes the contribution from the sclera, resulting in the observation of increased S/N of collagen. Averaged SORS spectra measured

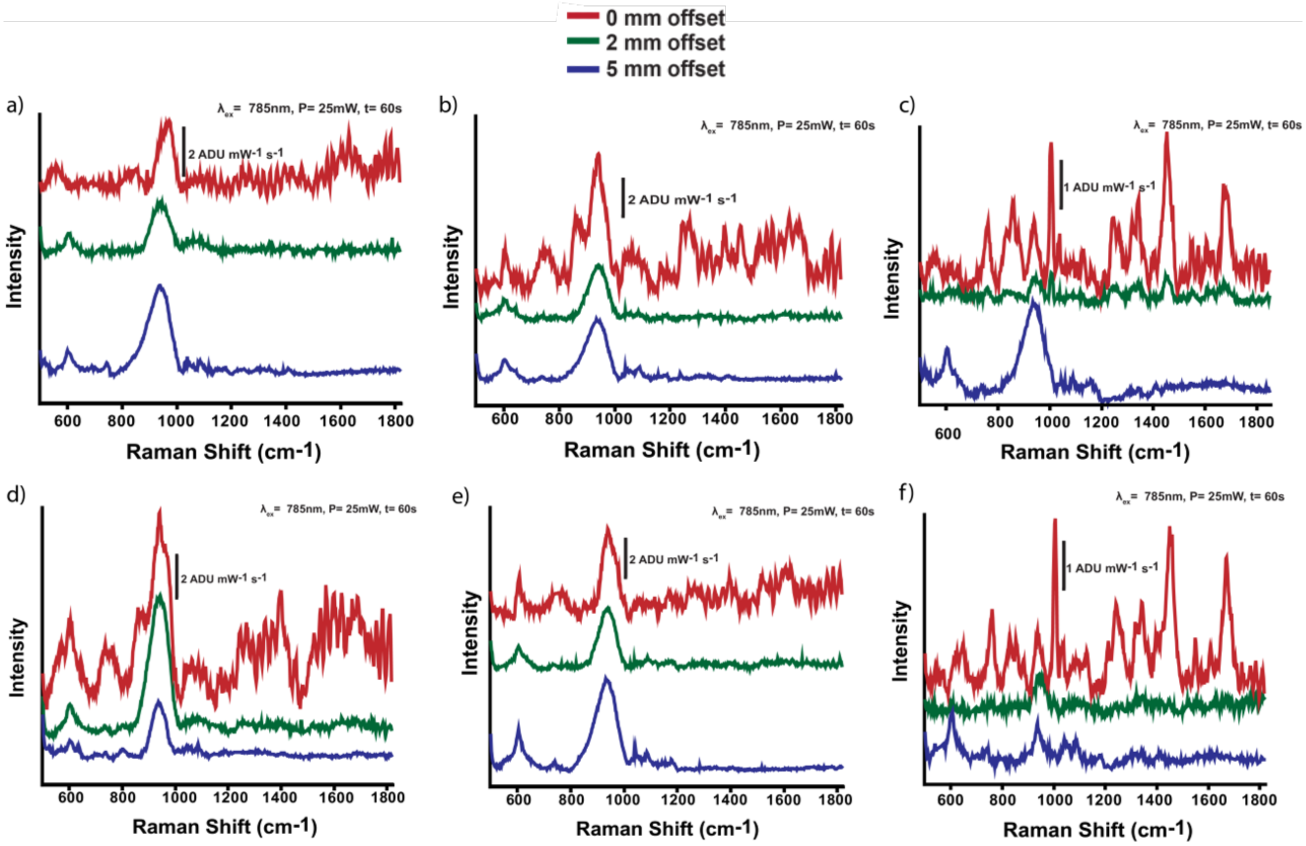

Figure 13. Average SORS Spectra. Average spectra from eye 1 (a-c) and eye 2 (d-f). Specrea were measured through the back (a and d), side (b and e), and front (c and f) of the eye at 0, 2, and 5mm offsets.

through the front of the eye show that there are several peaks measured in the 0mm offset that are not measured in the other offsets. The peak around 939 cm^{-1} is measured in all offsets and is again attributed to collagen. Several other peaks are seen in the 0mm offset spectra, including peaks around 758 cm^{-1}, 831 cm^{-1}, 855 cm^{-1}, 883 cm^{-1}, 1005 cm^{-1}, 1034 cm^{-1}, 1241 cm^{-1}, 1341 cm^{-1}, 1450 cm^{-1}, 1550 cm^{-1}, and 1669 cm^{-1}. Peaks at 1005 cm^{-1} and 1450 cm^{-1} were found in the 0 and 2mm offsets through the front of the eye. To determine where these peaks were arising from, spectra from the lens alone were analyzed and a representative spectrum is shown in Figure 14. It can be seen that many of the peaks observed in the 0mm offset spectra are arising from the lens, indicating that using Raman with no offset allowed for the observation of lens through the cornea. It is thought that because of the transparency of the cornea, the laser focused straight through the cornea onto the lens. It is well known that the eye lens is comprised of crystalline proteins. This indicates that the peaks observed are due to proteins. Based on literature, several of the peaks in the lens spectra were assigned and summarized in Table 1. [10, 16] Peaks from the lens were also found in the 2mm offset spectra, so we concluded that we had not fully passed the lens with the 2mm offset. It is noted that the lens peaks are not observed at the 5mm offset. If more studies were to be done, it would be worth studying different depths to determine which offset best focuses on the lens. Future work should include using multiple other offsets to determine if more chemical differences at different depths of the eye can be noted and utilized for diagnostic

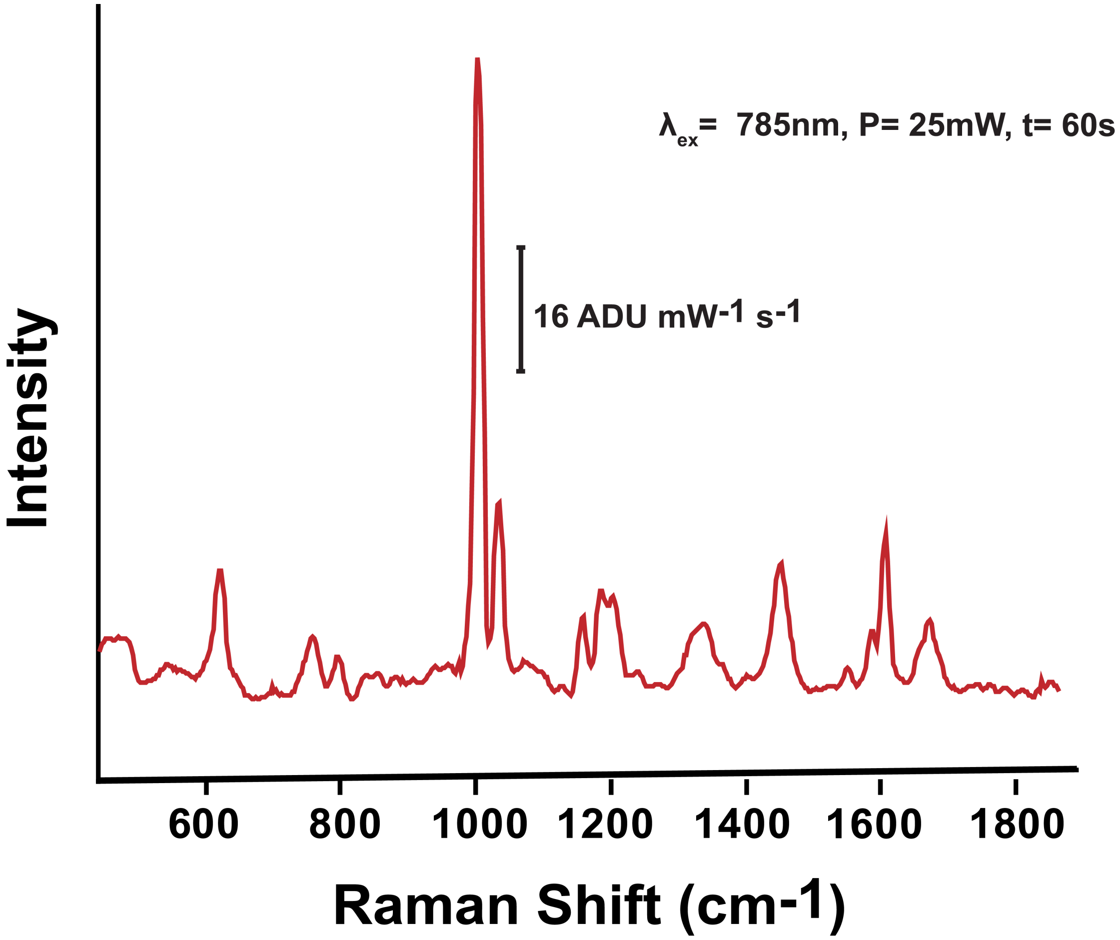

Figure 14. Raman Spectrum of Bovine Lens. Lens spectrum collected at 785-nm excitation, 25mW power, with acquisition time of 60 seconds.

Table 1: Peak Assignments of Lens

Component	**Peaks (cm^{-1})**
Tryptophan	758, 880
Tyrosine	834, 855
Phenylalanine	1005, 1032
Protein peaks	1340, 1450,1550, 1669

purposes. As this study was just preliminary, more eyes should be studied to show that this is indeed reproducible in different samples.

3.4 Conclusions and Future Work

In conclusion, we were able to use SORS to measure through different parts of whole bovine eyes non-invasively. Spectra were found to be representative of the components known to be in each part of the eye. It was shown that a 0mm offset through the front of the eye results in a Raman spectrum where several peaks are attributed to the lens proteins, and the 2mm spectrum also shows some peaks attributed to the lens. It was shown that collagen can be measured through the back and side of the eye, with a 5mm offset giving the best S/N ratio. Measuring through the eye could be useful in non-invasively and non-destructively diagnosing diseases such as cataracts, macular degeneration, and glaucoma. This method should be studied in depth to determine optimum offsets for measuring through each part of the eye. The maximum power that could be applied to the eye without damaging it should also be studied. It is thought that measuring spectra of the lens over time could be a useful tool for disease diagnosis or forensic post-mortem interval analysis. In the future, this SORS method could be used to determine trends in chemical components that could be indicative of disease or of post-mortem interval.

3.5 References

1. Institute, N. E. Eye Disease Statistics. https://www.nei.nih.gov/sites/default/files/2019-04/NEI_Eye_Disease_Statistics_Factsheet_2014_V10.pdf (accessed 30 April 2020).

2. Girela, E.; Villanueva, E.; Irigoyen, P.; Girela, V.; Hernández-Cueto, C.; Peinado, J. M., Free Amino Acid Concentrations in Vitreous Humor and Cerebrospinal Fluid in Relation to the Cause of Death and Postmortem Interval. *Journal of Forensic Sciences* 2008, *53* (3), 730-733.

3. Patrick, W. J.; Logan, R. W., Free amino acid content of the vitreous humour in cot deaths. *Archives of Disease in Childhood* 1988, *63* (6), 660-662.

4. Munoz, J. I.; Costas, E.; Rodriguez-Calvo, M. S.; Suarez-Penaranda, J. M.; Lopez-Rivadulla, M.; Concheiro, L., A high-performance liquid chromatography method for hypoxanthine determination in vitreous humour: application to estimation of post mortem interval. *Hum Exp Toxicol* 2006, *25* (5), 279-81.

5. Thierauf, A.; Musshoff, F.; Madea, B., Post-mortem biochemical investigations of vitreous humor. *Forensic Science International* 2009, *192* (1-3), 78-82.

6. Yu, N. T.; East, E. J., Laser Raman spectroscopic studies of ocular lens and its isolated protein fractions. *J Biol Chem* 1975, *250* (6), 2196-202.

7. Yu, N.-T.; Kuck, J. F. R.; Askren, C. C., Laser Raman spectroscopy of the lens in situ, measured in an anesthetized rabbit. *Current Eye Research* 2009, *1* (10), 615-618.

8. Bot, A. C. C.; Huizinga, A.; de Mul, F. F. M.; Vrensen, G. F. J. M.; Greve, J., Raman microspectroscopy of fixed rabbit and human lenses and lens slices: New potentialities. *Experimental Eye Research* 1989, *49* (2), 161-169.

9. Sokolov, K. V.; Lutsenko, S. V.; Nabiev, I. R.; Nie, S.; Yu, N.-T., Surface-Enhanced Raman Analysis of Biomedical Eye Lens Extracts. *Applied Spectroscopy* 2016, *45* (7), 1143-1148.

10. Vrensen, G.; Otto, C.; Lenferink, A.; Liszka, B.; Montenegro, G. A.; Barraquer, R. I.; Michael, R., Protein profiles in cortical and nuclear regions of aged human donor lenses: A confocal Raman microspectroscopic and imaging study. *Exp Eye Res* 2016, *145*, 100-109.

11. Katz, A.; Kruger, E. F.; Minko, G.; Liu, C. H.; Rosen, R. B.; Alfano, R. R., Detection of glutamate in the eye by Raman spectroscopy. *J Biomed Opt* 2003, *8* (2), 167-72.

12. Prieto-Bonete, G.; Perez-Carceles, M. D.; Luna, A., Morphological and histological changes in eye lens: Possible application for estimating postmortem interval. *Legal Medicine* 2015, *17* (6), 437-442.

13. Matousek, P.; Clark, I. P.; Draper, E. R. C.; Morris, M. D.; Goodship, A. E.; Everall, N.; Towrie, M.; Finney, W. F.; Parker, A. W., Subsurface Probing in Diffusely Scattering Media Using Spatially Offset Raman Spectroscopy. *Applied Spectroscopy* 2016, *59* (4), 393-400.

14. Matousek, P., Inverse spatially offset Raman spectroscopy for deep noninvasive probing of turbid media. *Applied Spectroscopy* 2006, *60* (11), 1341-1347.

15. Matousek, P.; Clark, I. P.; Draper, E. R. C.; Morris, M. D.; Goodship, A. E.; Everall, N.; Towrie, M.; Finney, W. F.; Parker, A. W., Subsurface probing in diffusely scattering media using spatially offset Raman spectroscopy. *Applied Spectroscopy* 2005, *59* (4), 393-400.

16. Paluszkiewicz, C.; Chaniecki, P.; Rękas, M.; Rajchel, B.; Piergies, N.; Kwiatek, W. M., Analysis of Human Lenses by Raman Microspectroscopy. *Acta Physica Polonica A* 2016, *129* (2), 244-246.

CHAPTER IV
SORS FOR DETERMINATION OF BONE FRACTURE AGING

This chapter details the use of normal Raman and SORS to measure the chemical composition of bone in relation to its healing. Normal Raman and SORS were used to find ratios of different components that describe bone fracture healing such as the ratios of carbonate/phosphate, carbonate/amid I, phosphate/amide I, and the full-width half maximum (FWHM) of phosphate. These ratios each tell something about the healing bone, and we aimed to show how bone heals over time in the intervals of 1 month, 3 months, 6 months, 9 months, and 12 months.

A version of this chapter will be prepared for submission in Fall of 2020.

4.1 Abstract

Knowledge of the microscopic, physical, and chemical properties of bone formation can give insight into how fractured bones will heal or have healed over time. It is known that Raman spectroscopy to ascertain chemical ratios (matrix/bone, etc.) provide valuable information about bone properties. It is also known that bone heals in stages, although it is not well known what the chemical composition is at each stage of bone haling. To address this gap in knowledge, we used normal Raman and SORS to show that fractured bone does change in composition as it heals, and ratios may be able to be used to determine the trends in bone healing in order to monitor it in real time also to one day help to accurately estimate the age of a bone fracture, especially for application to child abuse cases. The overall objective was to establish the chemical composition of fractured bone at different stages in the healing process and apply this toward in vivo monitoring of bone in real time. It was discovered that ratios change over time and could prove to be valuable in determining what stage of healing the fracture is in.

4.2 Introduction

It is well known that bone tissue is made of two phases, the carbonated apatite mineral phase, which contains mineral phosphate and carbonate and the organic matrix phase, which contains Type I collagen. [1,2] It is also recognized that Raman spectroscopy can be used to determine the composition of bone. Figure 15 shows the Raman spectrum of bone. Raman peaks that describe the matrix include hydroxyproline (876 cm^{-1}), proline (921 and 855 cm^{-1}), phenylalanine (1002 cm^{-1}), amide III (1250 cm^{-1}), CH_2 wag at 1447 cm^{-1}, and the amide I band at 1667 cm^{-1}. Several Raman peaks describe the mineral (inorganic) portion of the bone. These include the phosphate peak around 959 cm^{-1} and carbonate around 1070 cm^{-1}. Ratios of peaks seen in the Raman spectra of bones reveal crucial information about the bone, described in Table 2.

Table 2: Ratios of bone peaks as described by Morris et al.[1]

Chemical Ratio	**Description**
Phosphate (959 cm^{-1})/Amide I (1616-1720 cm^{-1})	Indicates amount of mineralization
Carbonate (1070 cm^{-1})/Phosphate (959 cm^{-1})	Varies with bone architecture, age, and crystallinity
Carbonate (1070 cm^{-1})/Amide I (1616 -1720 cm^{-1})	May indicate bone remodeling
FWHM of phosphate (959 cm^{-1})	Indicates degree of crystallinity

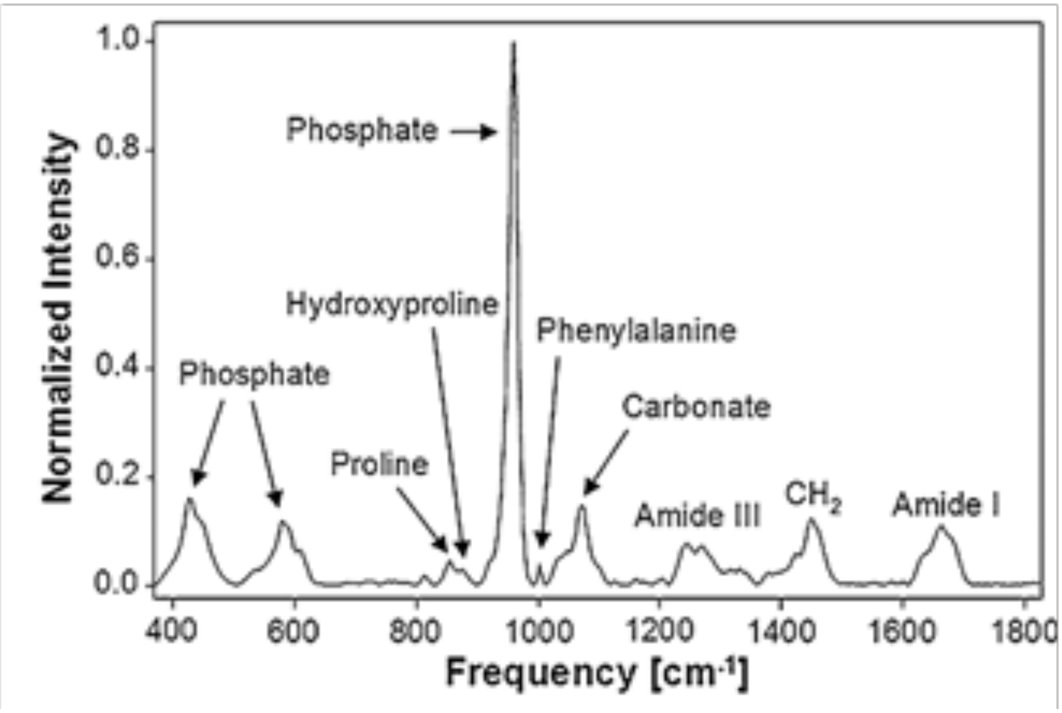

Figure 15. Raman Spectrum of Bone. Spectrum of 6 week old mouse bone at 785 nm, Reproduced from Morris et al.[1]

Raman spectroscopy has been used extensively to study bone composition and healing. Raman spectroscopy has previously been used to monitor the healing process in rat bones by Gamulin et al. [3] They studied the healing effect of stable gastric pentadecapeptide (BPC157) on rat femoral heads and discovered that there was a statistical difference between treated, control, and healthy animals indicating a positive influence of BPC on rat bone healing. Ding et al. has used spatially-offset Raman spectroscopy (SORS) to look at bone fractures in rat bones. [4] In this study, it was observed that the phosphate band at 960 cm^{-1} was weaker in fractured bone, which meant there was less mineralization in the femur that had been fractured. Hydroxyapatite, proline, and carbonate are directly related to the relative amount of mineral and collagen, so the peak height ratios of phosphate/proline, carbonate/phosphate, and proline/amide III were used to determine the extent of collagen mineralization, carbonation, and collagen content, respectively. [4] Feng et al. showed that SORS is promising for measuring chemical differences in subcortical bone tissue. [6] The ability of SORS to measure through bone was analyzed by putting a known substance, Tylenol, behind bone and measuring normal spectra at 0 mm and an offset. Tylenol was seen better at an offset, indicating subcortical tissue can be measured using SORS. They then studied murine bones with and without osteoporosis and observed a noticeable difference, leading to the conclusion that normal and diseased bone are different from one another.

In our study, normal Raman and SORS was used to analyze bone fracture healing at different time intervals ranging from 1 to 12 months. The main hypothesis was that chemical ratios shown in Table 2 would change over time. We expected changes in the mineral and organic contributions to Raman spectra at different intervals of healing. We expected that as a bone heals, more mineral is deposited and bone ratios as well as phosphate content discussed in Table 2 will change due to bone mineralization and remodeling.

4.3 Materials and Methods

Goat tibias from 5-year old goats that had been used in a previous study were obtained from the University of Tennessee Veterinary School. Animals were sacrificed humanely by trained veterinarians at the respective month interval. For this work, only controls were used, meaning samples had not been treated with drugs and any healing present was natural. We obtained available control samples including: one 1-month sample, one 3-month sample, four 6-month samples, seven 9-month samples, and four 12-month samples. Samples had been stored in a deep freezer at -80 degrees Celsius after collection. Samples were thawed on ice before use, and as much blood as possible removed using 3% hydrogen peroxide. Any excess tissue was removed using dissection tools.

A microscope at 20X magnification equipped with a camera was used to image bones near and far from the fracture line on a bone of each month time interval. The spot was focused on the bone by first focusing with the microscope, and then a picture was taken at the spot with 20X magnification. Images were taken at points both near and far from the fracture on each bone in order to see microscopic structural differences.

After images were collected on the microscope, bones were subjected to spatially offset Raman spectroscopy (SORS). The home-build macro-Raman system seen in Figure 8, equipped with a 785-nm laser at 25 mW of power. Raman spectra of the bones were collected from each bone at 2-6 spots (depending on size of the bone) on each side (proximal or distal) of the bone. Bone thicknesses were measured with a micrometer and ranged from 3-10 mm. For SORS spectra, offsets were determined by this thickness, with the offset being approximately half the thickness of the bone.

To obtain chemical information from the bones, normal RS spectra of each bone were taken at each point depicted in Figure 16 at 0 mm offset and an offset determined by choosing an offset of half the thickness of the bone. Collection of data from each spot (both no offset and offset) consisted of three frames with 60 seconds of acquisition time each. Bones had previously been cut along the sagittal plane, which allowed for the collection of what would normally be the inside of the bone, with the 0mm offset focusing on the inside part of the bone. We collected data from this site of the bone in order to directly measure Raman spectra at the innermost part of healing.

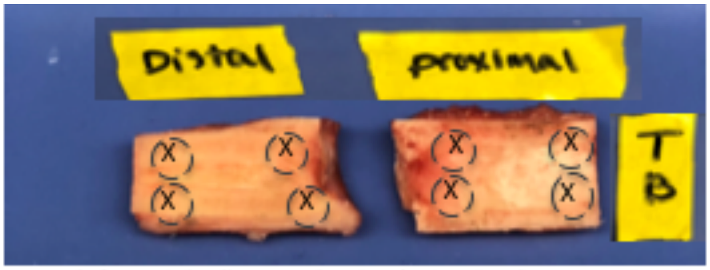

From left to right (bottom): Distal B2, Distal B1, Proximal B2, Proximal B1
Left to right (top):Distal T2, Distal T1, Proximal T2, Proximal T1

Figure 16. Locations of Data Collection. Data was collected at each spot, with the x representing the 0 mm offset (no offset) and the circle representing an offset.

Spectra were preprocessed by baseline correction and smoothing using home-written MatLab code. Spectra were then peakfit with GRAMS/AI software (ThermoScientific). An example of this is shown in Figure 17. Peak fitting allowed for determining the integrated peak areas for the major components of bone. After peak-fitting each spot of the bone, data was normalized. To normalize data, the data from the non-fractured part of the bone was first peak-fit and averaged. It was seen that the phenylalanine peak at approximately 1002 cm^{-1} remained the most constant between samples, and there is no evidence of changes in phenylalanine concentration with healing in the literature, so we chose to normalize to the phenylalanine peak. After peakfitting the normal bone data, the spectra near the fracture were peak-fit. Then normalization factors were calculated for each spot away from the fracture and spectra were normalized by dividing by the normalization factor. Normalized spectra were then peakfit and integrated areas of major components of bone were calculated. These areas were then used to calculate the ratios previously shown in Table 2.

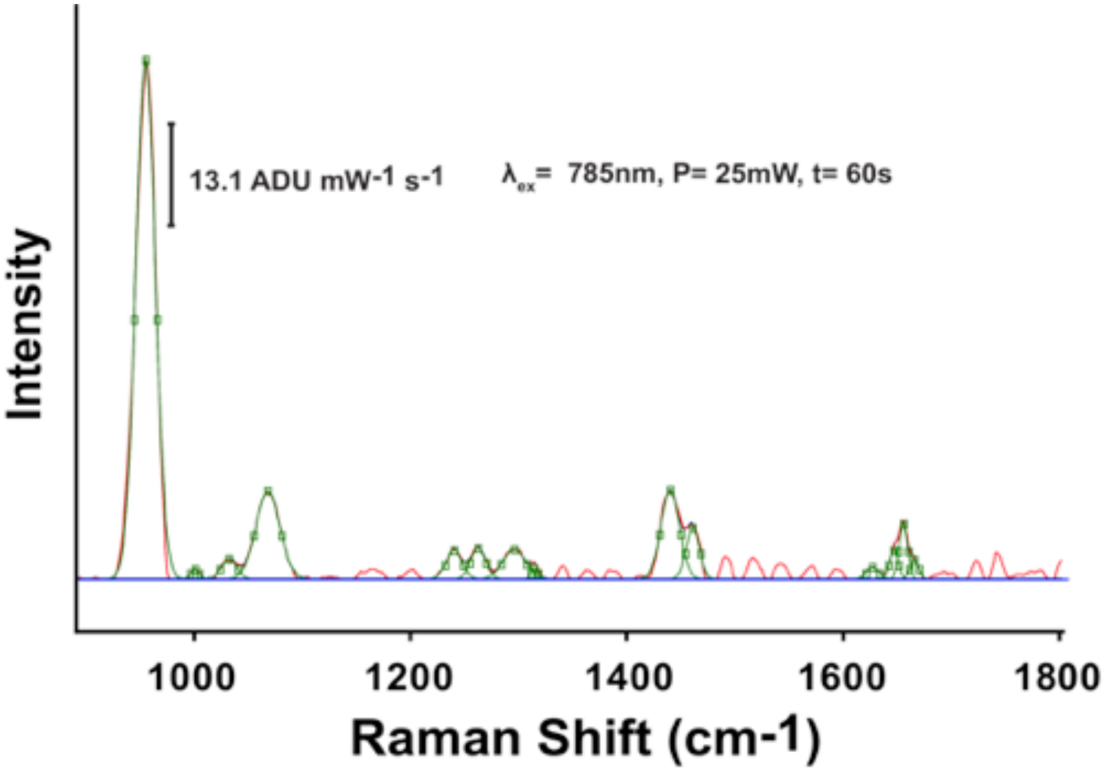

Figure 17. Peak-Fit Spectrum. Example of how spectra were peak-fit. Peaks were in Gaussian shape and areas calculated, which were then used to calculate ratios.

Statistics were used to determine significant differences in data. One-way analysis of variance (ANOVA) tests are used when determining if there are statistically significant differences between the means of 2 or more independent groups. This test was used in this study to determine statistically significant differences between the means of the 1,3,6,9, and 12- month samples. ANOVAs were performed in Statistical Product and Service Solutions (SPSS) for each of the four chemical ratios at each bone location (distal near side, distal far side, proximal near side, proximal far side). The detailed results of these ANOVAs can be found in the Appendix.

ANOVA testing only tells that there is a difference and not where the difference lies between samples, therefore, a post-hoc test is necessary to establish which samples were statistically different. For this test, we utilized the Tukey honest significant difference, also carried out by SPSS software. The Tukey test compares differences between means of values and identifies where there are significant differences. Differences were considered significant when $p < 0.05$.

4.4 Results and Discussion

Figure 18 shows photos taken on the microscope both near and far from the fracture site. Visible differences are observed between the structure of normal and fractured bone on a microscopic scale. Particularly, it is seen that the 6-month bone looks more like a webbed structure near the fracture than the structure of normal bone. It was concluded that bone near the fracture line looks more like woven bone than lamellar bone, which is reasonable because woven bone is characteristic of bone remodeling. Woven bone is the first bone laid down after a fracture and is characterized by collagen fiber. The woven bone is gradually replaced by lamellar bone, so it would be reasonable to see woven bone in the fractured areas of the bone.[6] Although microscope images provided some information about the bone structure, they did not provide quantitative information, so it was determined that chemical information would be beneficial in understanding what is happening at a molecular level that could differentiate between normal and fractured bone.

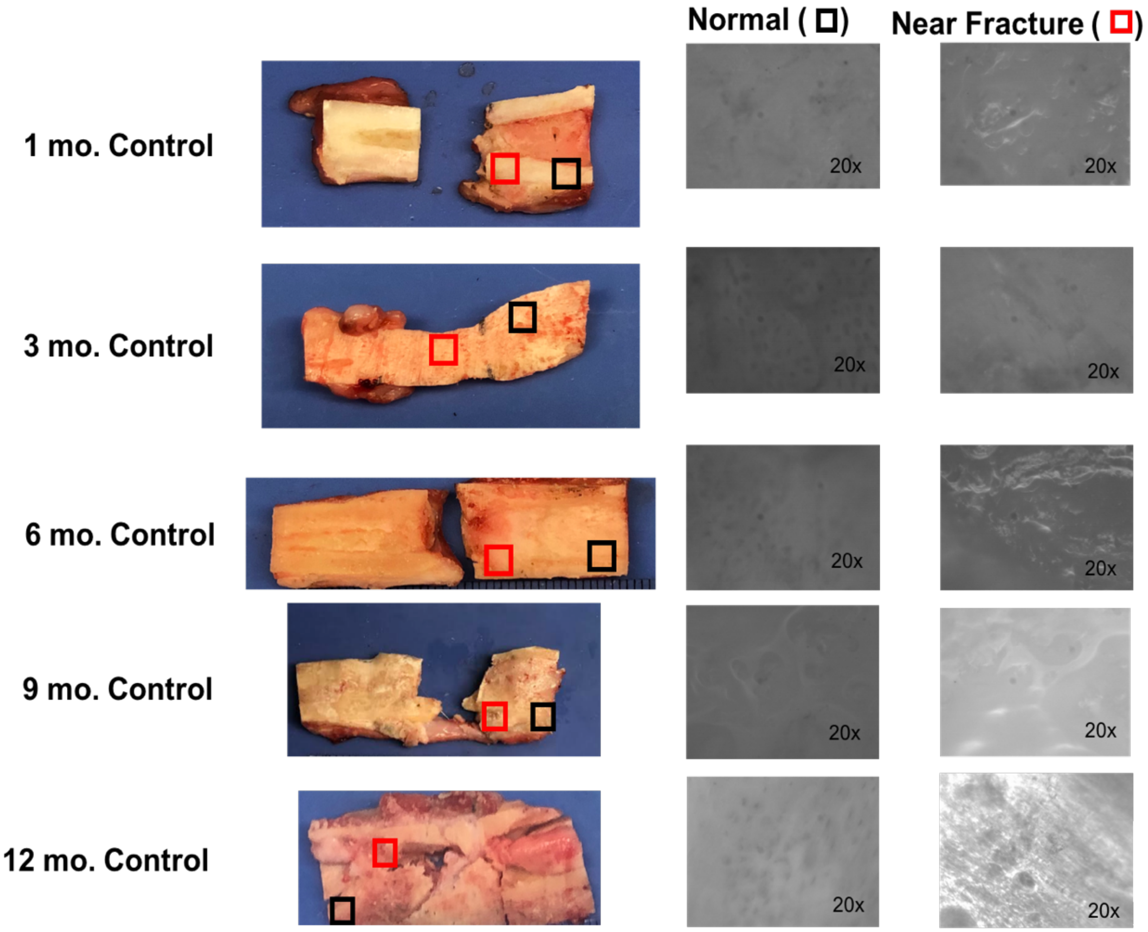

Figure 18. Photos of normal and fractured goat tibia samples. The boxes indicate spots where the magnified images were collected on the normal bone and near fractured bone. Magnification of 20X.

Average chemical ratios from normalized spectra are depicted in Figures 19-22. Pooled standard deviations (see Appendix) are shown by error bars, calculated based on how many frames of data had been averaged for that month's interval. Figure 19a shows that on the side near to the fracture on the distal bones, phosphate/amide I ratio increased at 6 months, decreased again at 9 months, and then slightly increased at 12 months, and on the far side of the bone, there was an initial decrease, then an increase at 6 months, and then a continued decrease in phosphate/amide I. At 6 months, the ratio was interesting similar in the near and far sides of the distal bones.

In order to determine if these trends were significant, an analysis of variance (ANOVA) was conducted on each part of the bone (distal far side, distal near side, proximal far side, proximal near side) to determine if the changes seen between months were significant. The ANOVA of the far distal side of the bone for the phosphate/amide I ratio was ($F(4,18)=10.884, p=0.000$) and the ANOVA for the near side of the distal bone was ($F(4,18)= 3.692, p=0.023$) indicating there were significant differences between months on both sides of the distal bone. To further determine where the differences lie, a Tukey test (Tukey's Honest Significant Difference test) was conducted. The Tukey test showed, as seen in Figure 19, that there was a significant change between 1 and 3 months ($p=0.005$), 6 and 12 months ($p=0.015$), 1 and 9 months ($p=0.001$), and 1 and 12 months ($p<0.001$) for the far side of the distal bone, indicating changes seen in phosphate/amide I ratio were significant. There was also a significant difference between 6 and 9 months (p=0.018) for the near side of the distal bone, indicating a significant change in mineralization.

Figure 19b shows the phosphate/amide I ratio trend for the proximal side of the bone. On the near fracture side of the proximal bone, there was a steady decrease of phosphate/amide I ratio through the 12 months. On the far side of the proximal bones, there was a decrease from 3 to 6 to 9 months, and then an increase. Again, around 6 months the ratios were near the same. After conducting an ANOVA for both near and far sides of the proximal (F(4,18)=2.444, p=0.084) and (F(4,16)=1.068, p=0.404), respectively, it was determined that there were no significant differences on the proximal side of the bone, although there did seem to be a decrease in phosphate/amide I ratio over time. Based on the trends observed here, it can be determined that phosphate/amide I ratio changes as bone heals, indicating changes in mineralization, with significant changes occurring in distal side of the bone.

a) Distal

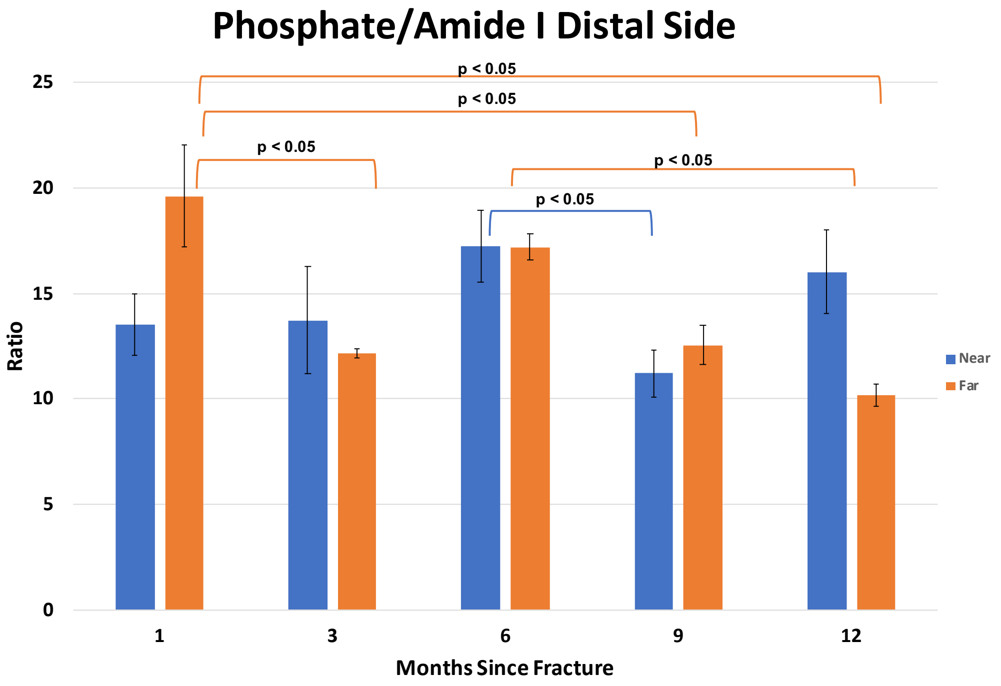

b) Proximal

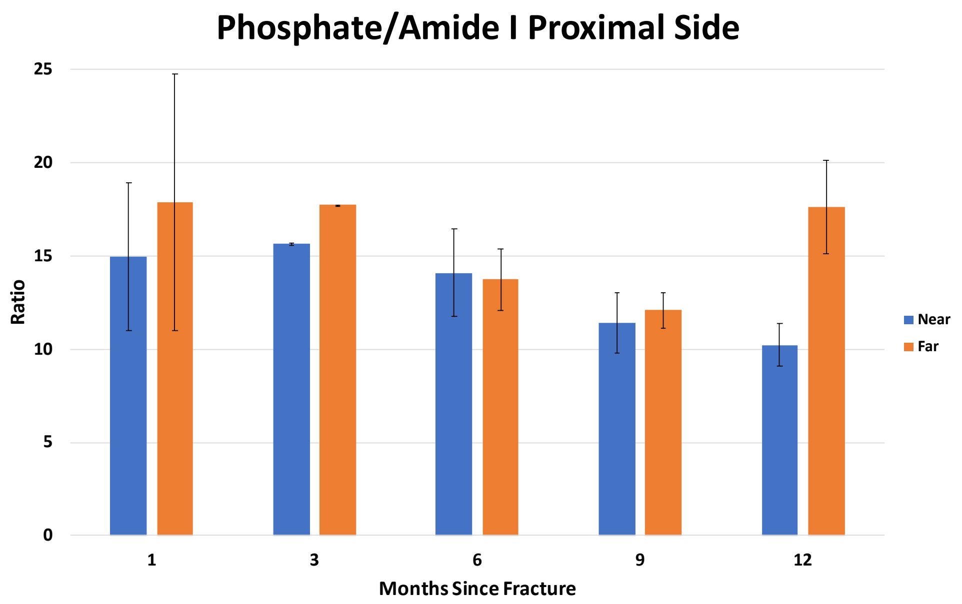

Figure 19. Average Phosphate/Amide I Ratio Over Time. Average phosphate (960 cm^{-1})/Amide I (1660 cm^{-1}) ratios of normalized, peakfit data per month. A) Distal side shows the trend over the 12 months for the distal side of the bone and B) Proximal shows the trend over 12 months for the proximal side of the bone. Significant differences ($p<0.05$) shown by brackets corresponding to near (blue) or far (orange) side.

Figure 20a shows that on the side near to the fracture on the distal bones, carbonate/phosphate ratio slightly increased at 3 months, then decreased over time. On the far side of the bone, there was an initial increase, then a decrease between 3 and 9 months, and then a sharp increase at 12 months, indicating the architecture of the bone at 12 months on the far side was different than the near side, having more carbonate to phosphate. The ANOVA for the carbonate/phosphate ratio on the far side of the distal bone indicated a significant difference between months (F(4,18)= 5.154,p=0.006). As seen in Figure 20a, Tukey test indicated the significant difference between months was found between 1 and 3 months (p=0.048), 6 and 12 months (p=0.05), 9 and 12 months (p=0.05), and 1 and 12 months (p=0.01) on the far side of the distal bone. An ANOVA test of the near side of the distal bone indicated a significant difference between months (F(4,18)= 3.091,p=0.042). The Tukey test indicated a significant difference between 3 and 12 months (p= 0.05).

Figure 20b shows the carbonate/phosphate ratio trend for the proximal side of the bone. On the near fracture side of the proximal bone, there was an initial decrease at 3 months, and then an increase from 6 to 9 months, and a very slight decrease at 12 months. The end ratio on the near side of the proximal bone was slightly lower than the initial ratio, but not greatly changed. The end ratio on the far side of the proximal bone was lower than the initial ratio at 1 month. On the near distal side, there was a decrease in this ratio overall, but as opposed to the far proximal side, the far distal side had increased in this ratio.

ANOVAs of the near and far sides of the proximal bone (F(4,18) = 0.555, p=0.698) and (F(4,16)=0.732, p=0.583) indicated no significant differences between months in the proximal side of the bone. These results would indicate that the proximal and distal sides could be different from each other and this would require further investigation. It could be determined that there is, however a slight decrease in the carbonate/phosphate ratio near the fracture over time in both sides of the bone, with significant differences being observed in the distal side of the bone.

Figure 21a shows that on the side near to the fracture on the distal bones, carbonate/amide I ratio clearly decreases at 6 and 9 months and increases again at 12 months. The same trend is true for the far side of the bone. ANOVAs of the near and far sides of the bone indicated significant differences, with (F(4,18) = 11.547,p<0.000) and (F(4,18)=10.168,p<0.000), respectively. A Tukey test of the near side of the bone indicated a significant difference between 6 and 9 months (p=0.013), which is of particular interest in this study, as remodeling is thought to occur around 6 to 9 months and carbonate/amide I is indicative of remodeling. The Tukey test also indicated a significant difference between 3 and 12 months (p=0.017), indicating remodeling had taken place during this time.

On the proximal side of the bone, shown in Figure 21b, there was a clear decrease in the carbonate/amide I ratio over time on both the near and far sides of the bone. ANOVAs of the far and near sides of the proximal bone indicated no significant difference on the far side (F(4,16) = 2.891,p=0.056), and a significant

a) Distal

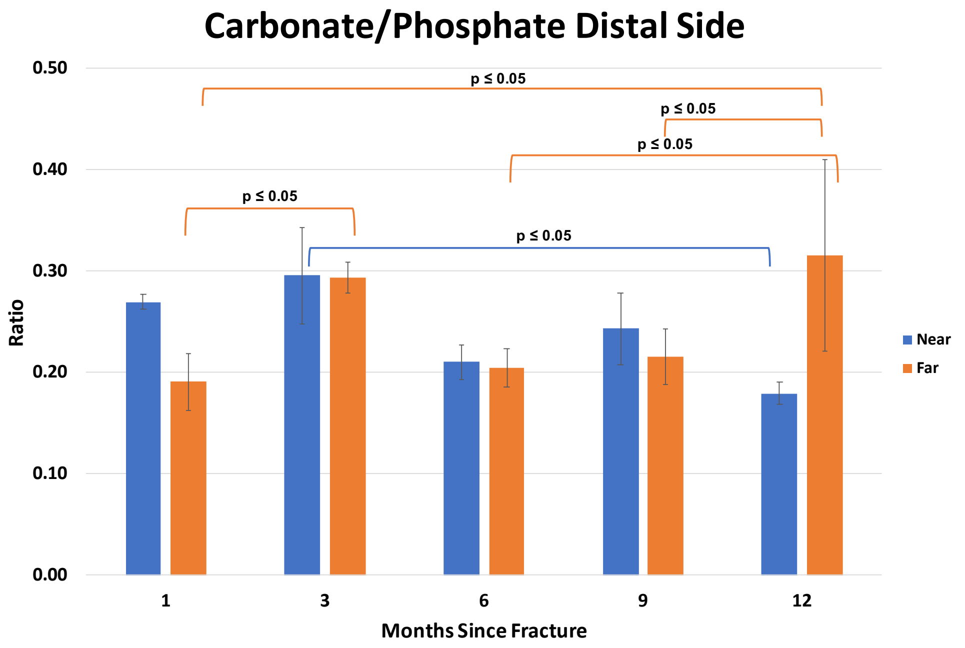

b) Proximal

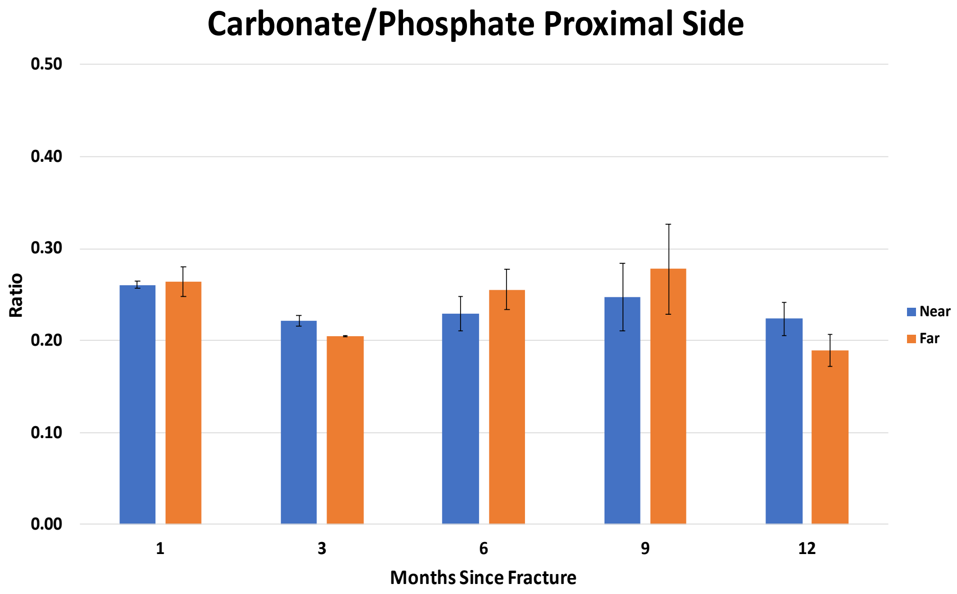

Figure 20. Average Carbonate/Phosphate Ratio Over Time . Average carbonate (1070 cm^{-1}) /phosphate (960 cm^{-1}) ratios of normalized, peakfit data per month. **A) Distal** shows the trend over the 12 months for the distal side of the bone and **B) Proximal** shows the trend over 12 months for the proximal side of the bone. Significant differences (p<0.05) shown by brackets corresponding to near (blue) or far (orange) side.

difference between months on the near side (F(4,18) =6.148, p=0.003). The Tukey test of the proximal near side indicated the significant difference was between 1 and 9 months (p=0.004) and 1 and 12 months (p=0.013). The trends observed here indicate that there is a decrease in carbonate/amide I ratio as bone heals, and this could be the most optimal ratio to use to estimate age of a fracture, as there is a clear decrease at 6-9 months on the distal side, which is where remodeling is thought to occur.

Figure 22a shows that on the side near to the fracture on the distal bones, the FWHM of phosphate does not change too much, although there is a slight increase in the near side at 3 months, and a decrease in the far side at 3 months. ANOVAs of the near and far sides of the distal bone indicate a significant difference on the far side (F(4,18) =5.240,p=0.006) and no significant difference on the near side of the distal bone (F(4,18) =2.037,p=0.132). The significant differences on the far side were found by the Tukey test to be from 1 to 3 months (p=0.026) and 1 to 12 months (p=0.011). These results indicate there was a significant change in crystallinity on the far side of the distal bone and no significant change in crystallinity on the near side.

In the proximal side of the bone, shown in Figure 22b, there is an increase in both the near and far side at 3 months and then a steady slight decrease. ANOVAs of the near and far sides of the proximal bone indicated significant differences between months on both near and far sides of the proximal bone with (F(4,18)=10.6222,p<0.000) and (F(4,16) =3.127,p=0.044), respectively. Tukey

a) **Distal**

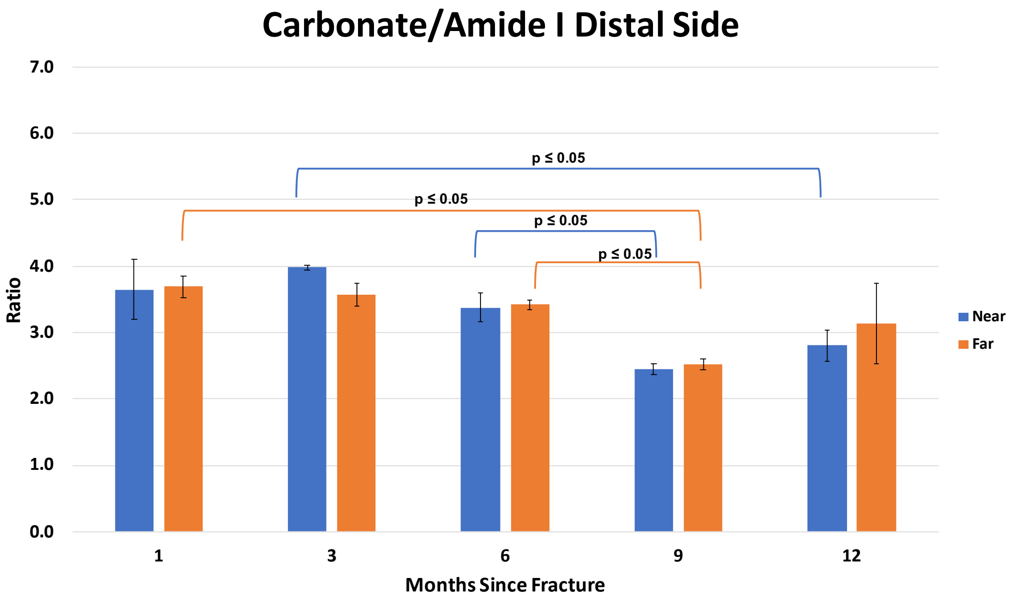

b) **Proximal**

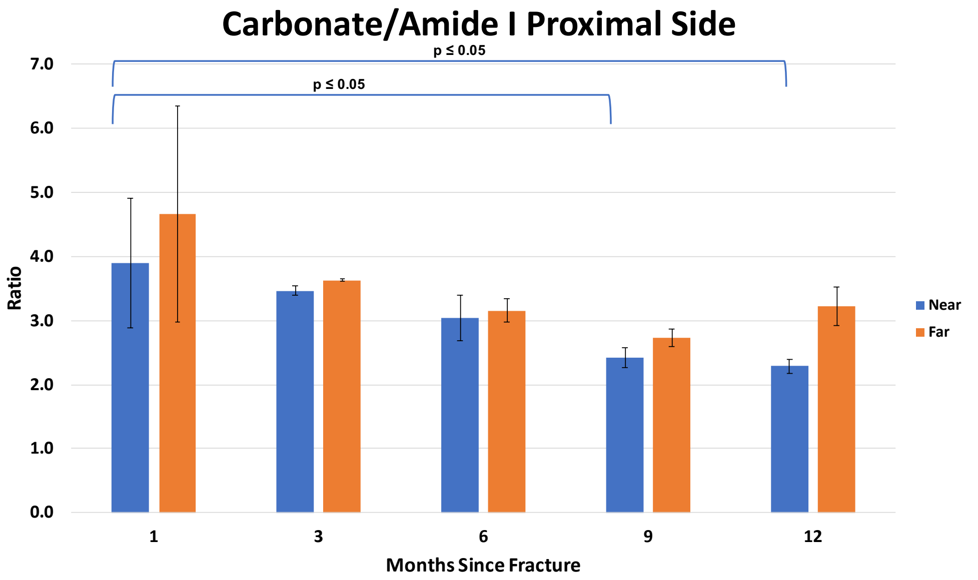

Figure 21. Average Carbonate/Amide I Ratio Over Time. Average carbonate (1070 cm^{-1})/Amide I (1660 cm^{-1}) ratios of normalized, peakfit data per month. A) Distal side shows the trend over the 12 months for the distal side of the bone and B) Proximal shows the trend over 12 months for the proximal side of the bone. Significant differences (p<0.05) shown by brackets corresponding to near (blue) or far (orange) side.

tests indicated that on the near side of the proximal bone, statistically significant differences were observed from 1 to 3 months (p=0.004), 3 to 6 months (p=0.041), and 1 to 12 months (p=0.048). On the far side of the proximal bone, the Tukey test indicated a statistically significant difference from 3 to 12 months (p=0.027). These results indicate that on the proximal side of the bone, there were statistically significant changes in crystallinity over time.

4.5 Conclusions and Future Work

It is clearly shown here that there are chemical changes over time in bone that has been fractured. The phosphate/amide I ratio showed changes over time, with both the proximal and distal sides showing a decrease around 6 months, indicating the mineral to matrix ratio is lower at this time. This result supported that remodeling may be occurring at 6 months. The carbonate/phosphate ratio showed us that there were changes, but the proximal and distal sides seemed to be different from each other, and there were no significant differences on the proximal side. This could lead the way into new investigations as to if the proximal and distal sides of the bone are indeed different in their carbonate composition. The carbonate/amide I ratio showed a similar trend in both the proximal and distal sides of the bone, with a statistically significant difference occurring between 6 and 9 months on the distal side. This showed that there was remodeling taking place, and we expect that the carbonate/amide I ratio would be best for estimating age of fracture. The FWHM did not change drastically over time, but there was a statistically significant change in crystallinity proximally.

a) Distal

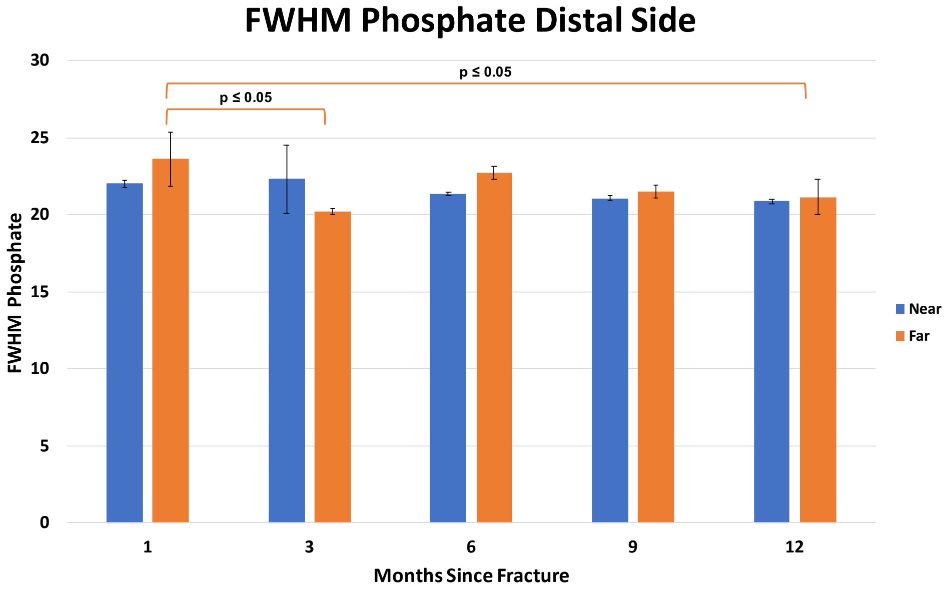

b) Proximal

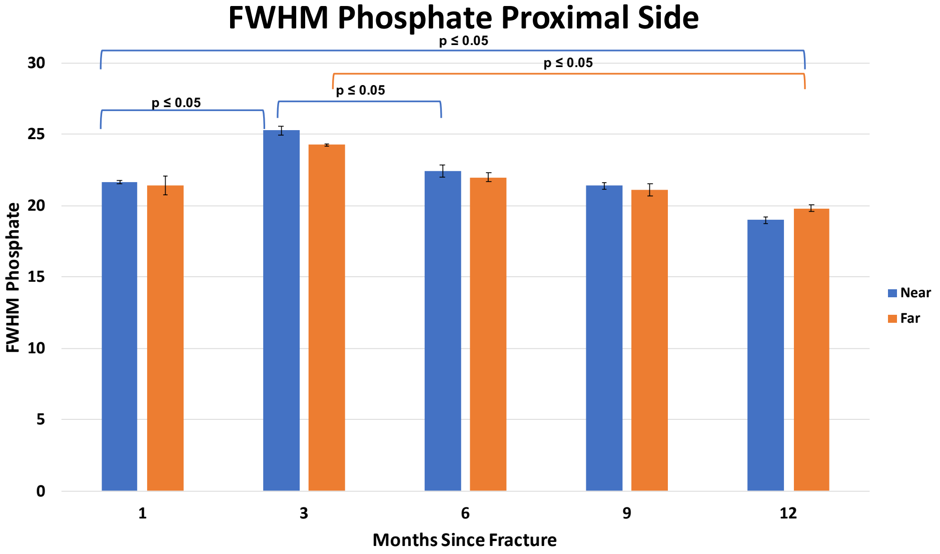

Figure 22. Average FWHM Ratio Over Time. Average full width at half maximum values of the phosphate (960 cm^{-1}) peak of normalized spectra at different months **A) Distal** shows the trend over the 12 months for the distal side of bones and **B) Proximal** shows the trend over the 12 months for the proximal side of the bone. Significant differences ($p<0.05$) shown by brackets corresponding to near (blue) or far (orange) side.

Table 3: Summary of statistically significant ratio differences between months

Chemical Ratio	Distal Side Significant Differences	Proximal Side Significant Differences
Phosphate (959 cm^{-1})/ Amide I (1616-1720 cm^{-1})	Far Side: 1 and 3 months 1 and 9 months 1 and 12 months 6 and 12 months Near Side: 6 and 9 months	None
Carbonate (1070 cm-^{1}) /Phosphate (959 cm^{-1})	Far Side: 1 and 3 months 6 and 12 months 9 and 12 months 1 and 12 months Near Side: 3 and 12 months	None
Carbonate (1070 cm^{-1})/ Amide I (1616 -1720 cm^{-1})	Far Side: 1 and 9 months 6 and 9 months Near Side: 6 and 9 months 3 and 12 months	Far Side: None Near Side: 1 and 9 months 1 and 12 months
FWHM of phosphate (959 cm^{-1})	Far Side: 1 and 3 months 1 and 12 months Near Side: None	Far Side: 3 and 12 months Near Side: 1 and 3 months 3 and 6 months 1 and 12 months

It may be noted that offset results have not been shown. Some results were processed, but the offset data showed that there was variability within a sample. We would need to further optimize the method in order to accurately use an offset to determine age of fracture. However, we were able to measure different chemical signals than the top layer using SORS so the theoretical use of SORS itself was validated. We also did not try to measure through the part of the bone that would be on layer just beneath the skin, so we would need to try to use SORS through that part of the bone. For this study’s purposes, it was shown that Raman and SORS can be used to describe the chemical composition of bone and bone changes in composition through the healing process. Future work would include further studying if the proximal and distal sides are different in their carbonate content and why, coming up with a better method of SORS to measure through bone using offsets, and creating a model based on chemical ratios.

4.6 References

1. Morris, M. D.; Mandair, G. S., Raman Assessment of Bone Quality. *Clinical Orthopaedics and Related Research®* **2010,** *469* (8), 2160-2169.
2. Morris, M. D.; Matousek, P.; Towrie, M.; Parker, A. W.; Goodship, A. E.; Draper, E. R. C., Kerr-gated time-resolved Raman spectroscopy of equine cortical bone tissue. *Journal of Biomedical Optics* **2005,** *10* (1).
3. Gamulin, O.; Serec, K.; Bilić, V.; Balarin, M.; Kosović, M.; Drmić, D.; Brčić, L.; Seiwerth, S.; Sikirić, P., Monitoring the healing process of rat bones using Raman spectroscopy. *Journal of Molecular Structure* **2013,** *1044*, 308-313.
4. Ding, H.; Lu, G.; West, C.; Gogola, G.; Kellam, J.; Ambrose, C.; Bi, X., Spatially offset raman spectroscopy for non-invasive assessment of fracture healing. In *Photonic Therapeutics and Diagnostics XII*, 2016.
5. Feng, G.; Ochoa, M.; Maher, J. R.; Awad, H. A.; Berger, A. J., Sensitivity of spatially offset Raman spectroscopy (SORS) to subcortical bone tissue. *Journal of Biophotonics* **2017,** *10* (8), 990-996.
6. Singh, A. P. Woven Bone and Lamellar Bone https://boneandspine.com/woven-bone-and-lamellar-bone/ (accessed February 6).

CHAPTER V.
CONCLUSION

As the technique of Raman spectroscopy is nondestructive, specific, and portable, it is desirable to forensic investigators, as it is imperative that evidence is preserved as best as possible. Raman spectroscopic techniques have begun to be widely used in the area of forensic science, although there is more research to be done into how else this method can be used in this field. The work presented here shows more ways Raman spectroscopy can be used to improve the field of forensic science.

First, we determined which biomarkers could be targeted using our surface enhanced Raman spectroscopy (SERS) method. We used both gold and silver nanoparticles to determine which would be optimum for studying the biomolecules of interest. It was determined that phenylalanine was likely the best target, as it gave a strong SERS signal with both instrumentation systems as well as both gold and silver nanoparticles. Phenylalanine has an easily detectable Raman spectrum, which would make this the analyte we would target first in biological systems. Tryptophan and tyrosine also gave a strong SERS signal, but they would need to be detected with AuNPs. Alanine and proline gave strong signal when detected using AgNPs on the macro-system. With AuNPs, less power is used and gold is less toxic than silver, leading to the conclusion that using AuNPs to measure amino acids, specifically phenylalanine, *in vivo* would be the logical choice to measure biomarkers of post-mortem interval. Future work in this area would include optimizing our SERS method with regards to nanoparticle parameters such as size and shape, pH, and time samples are incubated.

We were interested in studying biomarkers in the eye post-mortem in order to be able to study time since death or post-mortem interval (PMI). We successfully used SORS to measure through the eye. We were able to measure the spectra of the lens of the eye noninvasively by using a 0mm offset. The lens of the eye gave a distinctive Raman spectrum, with the phenylalanine peak being the most prominent. We measured through the front, side, and back of the eye using multiple different offsets. It was determined that to measure through the side and back of the eye, a 5mm offset was optimum because of its improved signal to noise ratio compared to the other offsets. Measuring through the eye could prove to be useful in not only determining time of death but also in diagnosing and evaluating eye disease such as glaucoma. Future work in this area would include collecting data from more samples and collecting data over time. The lens is of particular interest for determining post-mortem interval since it gives such a distinctive Raman spectrum. The lens would need to be studied over time to see how the phenylalanine and other peaks change. It is thought that a mathematical model of the phenylalanine change over time could be used to estimate time since death. This SORS method would also need to be implemented in a portable system and tried in the field.

We also studied how fractured bone composition changes as bones heal. We studied bones that had been previously fractured surgically and allowed to heal over 1,3,6,9, or 12 months. We collected normal Raman and SORS spectra on parts of the bone both near and far from the fracture and then normalized the data to the spots far from the fracture. After normalizing data, chemical ratios were calculated using peak areas. It was determined that chemical composition changes over time as bones heal. The phosphate/amide I peak ratio showed changes over time, with there being a decrease around 6 months in both the proximal and distal sides of the bone, indicating the mineral to matrix ratio is lower at this time, where bone remodeling is likely occurring. The carbonate/phosphate ratio showed that the proximal and distal side followed different trends. It would need to be investigated more to see if the composition is different on the opposite sides of the bone. The carbonate/amide I ratio is likely the best ratio to use to estimate age of fracture, as the carbonate/amide I ratio showed a consistent trend over time. As time went on, the carbonate/amide I ratio, which has previously been thought to be indicative of bone remodeling, decreased, and there was a statistically significant difference from 6-9 months, which is where remodeling is hypothesized to occur. It could be useful to mathematically model this decrease over time and create a model where a bone fracture of unknown age's carbonate/amide I ratio is determined and then the mathematical model used to predict the age of the fracture. The FWHM of phosphate showed little change in crystallinity over time, but there was a statistically significant change on the proximal side. Future work in this area would include developing a better method to use SORS through bone, measuring

SORS spectra through the side of the bone that would be under the skin normally, modeling this method using other species, and collecting data from more bone samples. Future work could also include collecting SORS spectra through the skin *in vivo* to determine chemical changes over time in a living organism. Ultimately, it would be desirable to create models to estimate age of fracture in both *in vivo* and *ex vivo* samples.

Overall, these investigations shed light into other ways SORS can be used in the forensics field. There is much method development to be completed, but these studies showed the versatility of SORS in this field and the promise it has to improve forensic investigation.

APPENDIX

STATISTICAL TESTING

Here we show the results from statistical testing of the bone samples in Chapter 4. Each location on the bone (distal near side, distal far side, proximal near side, proximal far side) was subjected to a one-way Analysis of Variance (ANOVA) test at alpha =0.05. The one and three month samples only had one sample, so data input into SPSS was from each frame of data. The ratios for each bone from the six, nine, and twelve month samples were calculated by the averages of the frames, and then the averages were calculated for each month interval. The data input into SPSS for the six, nine, and twelve month samples was the average of the average ratios of each month interval. Therefore, the standard deviation shown in the descriptives table does not show the pooled standard deviation, as was shown on the figures, but rather the standard deviation of the averages. Each ANOVA test is shown below. After ANOVA testing, samples were subject to a post-hoc test, the Tukey honest significant difference (Tukey HSD) test to see where significant differences lay in the data. The results of the Tukey tests are also shown below. Results were considered significant if $p<0.05$.

Table 1. Averaged data from bone samples, where n = number of frames. S.D is standard deviation; S.D. for 6,9, and 12 month samples are pooled standard deviations as there were multiple bones.

1 month Average									
Distal					Proximal				
AVERAGES	Near (n=6)	S.D.	Far (n=6)	S.D.	AVERAGES	Near (n=6)	S.D.	Far (n=6)	S.D.
Phosphate/AmideI	13.5111332	1.467088071	19.62154	2.427094067	Phosphate/Amide I	14.9553	3.9879	17.89162	6.871864
Carbonate/Phosphate	0.269760522	0.007739851	0.19077	0.027778703	Carbonate/Phosphate	0.2607	0.0042	0.263819	0.016037
Carbonate/Amide I	3.64902602	0.447180899	3.688978	0.166008635	Carbonate/Amide I	3.8935	1.0090	4.666903	1.689502
FWHM Phosphate	22.01137483	0.211439399	23.63317	1.75458053	FWHM Phosphate	21.6292	0.1246	21.43502	0.663503
3 month Average									
Distal					Proximal				
AVERAGES	Near (n=3)	S.D.	Far (n=3)	S.D.	AVERAGES	Near (n=3)	S.D.	Far (n=3)	S.D.
Phosphate/AmideI	13.72914296	2.53188447	12.14428	0.221117897	Phosphate/AmideI	15.64714768	0.059535492	17.72496	0.025434
Carbonate/Phosphate	0.295619168	0.047121037	0.293857	0.015040686	Carbonate/Phosphate	0.221488951	0.005334799	0.204783	0.001034
Carbonate/Amide I	3.979097135	0.035618404	3.56768	0.164497036	Carbonate/Amide I	3.465511527	0.07028793	3.629754	0.013126
FWHM Phosphate	22.33868133	2.225394061	20.24466	0.186762698	FWHM Phosphate	25.2735225	0.318887481	24.2618	0.079131
6 month Average									
Distal					Proximal				
AVERAGES	Near (n=24)	S.D.	Far (n=24)	S.D.	AVERAGES	Near (n=24	S.D.	Far (n=22)	S.D.
Phosphate/Amide I	17.22156509	1.698033816	17.19836	0.62796941	Phosphate/Amide I	14.10680161	2.337010243	13.72779	1.679247
Carbonate/Phosphate	0.210661098	0.017016157	0.204742	0.019225937	Carbonate/Phosphate	0.228725162	0.018615662	0.25516	0.022034
Carbonate/Amide I	3.377915027	0.218259723	3.421462	0.06924665	Carbonate/Amide I	3.038963689	0.360520532	3.158102	0.178825
FWHM Phosphate	21.36055208	0.138261039	22.76429	0.423074337	FWHM Phosphate	22.41055048	0.430269898	21.99719	0.319745
9 Month Average									
Distal					Proximal				
AVERAGES	Near (n=39)	S.D.	Far (n=37)	S.D.	AVERAGES	Near (n=36)	S.D.	Far (n=38)	S.D.
Phosphate/Amide I	11.20724864	1.120065453	12.55653	0.913046198	Phosphate/Amide I	11.42434853	1.609143326	12.08138	0.968405
Carbonate/Phosphate	0.24316339	0.034954637	0.215792	0.027605201	Carbonate/Phosphate	0.247251512	0.036790359	0.277599	0.049135
Carbonate/Amide I	2.448404161	0.085618522	2.525073	0.081642631	Carbonate/Amide I	2.427124162	0.152810534	2.729618	0.142633
FWHM Phosphate	21.07201576	0.14984499	21.52749	0.401424872	FWHM Phosphate	21.40351031	0.238322458	21.10993	0.423308
12 Month Average									
Distal					Proximal				
AVERAGES	Near (n=18)	S.D.	Far (n=17)	S.D.	AVERAGES	Near (n=15)	S.D.	Far (n=18)	S.D.
Phosphate/Amide I	16.03563042	1.96051888	10.18304	0.505544541	Phosphate/Amide I	10.23155845	1.135501216	17.61515	2.504877
Carbonate/Phosphate	0.17935339	0.010750408	0.315489	0.094130383	Carbonate/Phosphate	0.223583551	0.018220508	0.189054	0.017007
Carbonate/Amide I	2.805272248	0.235224573	3.133372	0.602543286	Carbonate/Amide I	2.291127475	0.109510852	3.220361	0.302566
FWHM Phosphate	20.87714628	0.149811392	21.1702	1.182184701	FWHM Phosphate	18.99292416	0.21896735	19.83083	0.266142

Distal Near Side

Table 2. Descriptive statistics of distal near side bone

						95% Confidence Interval for Mean			
		N	Mean	Std. Deviation	Std. Error	Lower Bound	Upper Bound	Minimum	Maximum
Phosphate Amidel	1	6	13.5111332	1.46708807	.59893620	11.9715187	15.0507477	12.01170	15.93037
	3	3	13.7291430	2.53188447	1.46178418	7.4395933	20.0186927	12.20976	16.65194
	6	4	17.2215651	4.82715760	2.41357880	9.5404801	24.9026500	11.02261	22.66513
	9	7	11.2072486	2.20739041	.83431515	9.1657530	13.2487443	6.84166	13.43266
	12	3	16.0356304	2.30255594	1.32938129	10.3157644	21.7554965	13.40374	17.67811
	Total	23	13.8129617	3.32153352	.69258762	12.3766229	15.2493006	6.84166	22.66513
Carbonate Phosphate	1	6	.2697605	.00773985	.00315978	.2616380	.2778830	.26004	.28069
	3	3	.2956192	.04712104	.02720534	.1785640	.4126743	.24128	.32528
	6	4	.2106611	.04234968	.02117484	.1432733	.2780489	.17713	.27243
	9	7	.2431634	.07225114	.02730836	.1763422	.3099845	.19191	.40177
	12	3	.1793534	.01862615	.01075381	.1330835	.2256233	.16203	.19905
	Total	23	.2429682	.05683915	.01185178	.2183891	.2675473	.16203	.40177
Carbonate Amidel	1	6	3.6490260	.44718090	.18256084	3.1797384	4.1183136	3.12350	4.30698
	3	3	3.9790971	.03561840	.02056430	3.8906161	4.0675782	3.94781	4.01786
	6	4	3.3779150	.59051212	.29525606	2.4382785	4.3175516	2.63838	3.97477

Table 2 Continued

	9	7	2.4484042	.22832241	.08629776	2.2372412	2.6595672	2.07768	2.77910
	12	3	2.8052722	.54038025	.31198868	1.4628933	4.1476512	2.18158	3.13342
	Total	23	3.1694675	.69094515	.14407202	2.8706805	3.4682546	2.07768	4.30698
FWHM Phosphate	1	6	22.0113748	.21143940	.08631977	21.7894828	22.2332669	21.72587	22.32624
	3	3	22.3386813	2.22539406	1.28483186	16.8104960	27.8668666	20.94707	24.90530
	6	4	21.3605521	.74255852	.37127926	20.1789758	22.5421284	20.71752	22.21432
	9	7	21.0720158	.56033410	.21178638	20.5537932	21.5902384	20.30127	21.91295
	12	3	20.8771463	.12972181	.07489492	20.5548994	21.1993931	20.75508	21.01336
	Total	23	21.5070457	.95111969	.19832217	21.0957507	21.9183407	20.30127	24.90530

Table 3. Analysis of Variance (ANOVA) output for distal near side bone

		Sum of Squares	df	Mean Square	F	Sig.
PhosphateAmideI	Between Groups	109.391	4	27.348	3.692	.023
	Within Groups	133.326	18	7.407		
	Total	242.717	22			
CarbonatePhosphate	Between Groups	.029	4	.007	3.091	.042
	Within Groups	.042	18	.002		
	Total	.071	22			
CarbonateAmideI	Between Groups	7.558	4	1.889	11.547	.000
	Within Groups	2.945	18	.164		
	Total	10.503	22			
FWHMPhosphate	Between Groups	6.202	4	1.550	2.037	.132
	Within Groups	13.700	18	.761		
	Total	19.902	22			

Table 4. Multiple comparisons test using Tukey HSD for distal near side

Tukey HSD

Dependent Variable	(I) Month	(J) Month	Mean Difference (I-J)	Std. Error	Sig.	95% Confidence Interval	
						Lower Bound	Upper Bound
PhosphateAmideI	1	3	-.21800976	1.92444746	1.000	-6.0371459	5.6011264
		6	-3.71043189	1.75677214	.258	-9.0225521	1.6016883
		9	2.30388456	1.51414716	.562	-2.2745873	6.8823564
		12	-2.52449722	1.92444746	.688	-8.3436333	3.2946389
	3	1	.21800976	1.92444746	1.000	-5.6011264	6.0371459
		6	-3.49242213	2.07864083	.470	-9.7778075	2.7929632
		9	2.52189432	1.87806842	.669	-3.1570010	8.2007897
		12	-2.30648746	2.22216052	.835	-9.0258471	4.4128721
	6	1	3.71043189	1.75677214	.258	-1.6016883	9.0225521
		3	3.49242213	2.07864083	.470	-2.7929632	9.7778075
		9	6.01431645*	1.70584035	.018	.8562036	11.1724293
		12	1.18593467	2.07864083	.978	-5.0994507	7.4713200
	9	1	-2.30388456	1.51414716	.562	-6.8823564	2.2745873
		3	-2.52189432	1.87806842	.669	-8.2007897	3.1570010
		6	-6.01431645*	1.70584035	.018	-11.1724293	-.8562036
		12	-4.82838178	1.87806842	.118	-10.5072771	.8505136

Table 4 Continued

	12	1	2.52449722	1.92444746	.688	-3.2946389	8.3436333
		3	2.30648746	2.22216052	.835	-4.4128721	9.0258471
		6	-1.18593467	2.07864083	.978	-7.4713200	5.0994507
		9	4.82838178	1.87806842	.118	-.8505136	10.5072771
CarbonatePhosphate	1	3	-.02585865	.03421177	.940	-.1293081	.0775908
		6	.05909942	.03123093	.356	-.0353365	.1535354
		9	.02659713	.02691768	.857	-.0547964	.1079907
		12	.09040713	.03421177	.104	-.0130423	.1938565
	3	1	.02585865	.03421177	.940	-.0775908	.1293081
		6	.08495807	.03695294	.190	-.0267801	.1966962
		9	.05245578	.03338727	.533	-.0485005	.1534121
		12	.11626578	.03950435	.059	-.0031873	.2357189
	6	1	-.05909942	.03123093	.356	-.1535354	.0353365
		3	-.08495807	.03695294	.190	-.1966962	.0267801
		9	-.03250229	.03032549	.818	-.1242004	.0591958
		12	.03130771	.03695294	.912	-.0804304	.1430458
	9	1	-.02659713	.02691768	.857	-.1079907	.0547964
		3	-.05245578	.03338727	.533	-.1534121	.0485005
		6	.03250229	.03032549	.818	-.0591958	.1242004
		12	.06381000	.03338727	.347	-.0371463	.1647663
	12	1	-.09040713	.03421177	.104	-.1938565	.0130423
		3	-.11626578	.03950435	.059	-.2357189	.0031873
		6	-.03130771	.03695294	.912	-.1430458	.0804304
		9	-.06381000	.03338727	.347	-.1647663	.0371463
CarbonateAmideI	1	3	-.33007112	.28603191	.776	-1.1949732	.5348310
		6	.27111099	.26111022	.834	-.5184330	1.0606550
		9	1.20062186*	.22504871	.000	.5201205	1.8811232
		12	.84375377	.28603191	.058	-.0211483	1.7086559
	3	1	.33007112	.28603191	.776	-.5348310	1.1949732
		6	.60118211	.30894978	.330	-.3330189	1.5353831
		9	1.53069297*	.27913856	.000	.6866350	2.3747510
		12	1.17382489*	.33028120	.017	.1751220	2.1725278

Table 4 Continued

	6	1	-.27111099	.26111022	.834	-1.0606550	.5184330
		3	-.60118211	.30894978	.330	-1.5353831	.3330189
		9	.92951087*	.25354019	.013	.1628571	1.6961646
		12	.57264278	.30894978	.376	-.3615583	1.5068438
	9	1	-1.20062186*	.22504871	.000	-1.8811232	-.5201205
		3	-1.53069297*	.27913856	.000	-2.3747510	-.6866350
		6	-.92951087*	.25354019	.013	-1.6961646	-.1628571
		12	-.35686809	.27913856	.707	-1.2009261	.4871899
	12	1	-.84375377	.28603191	.058	-1.7086559	.0211483
		3	-1.17382489*	.33028120	.017	-2.1725278	-.1751220
		6	-.57264278	.30894978	.376	-1.5068438	.3615583
		9	.35686809	.27913856	.707	-.4871899	1.2009261
FWHMPhosphate	1	3	-.32730650	.61689120	.983	-2.1926595	1.5380465
		6	.65082275	.56314205	.775	-1.0520038	2.3536493
		9	.93935907	.48536740	.335	-.5282928	2.4070110
		12	1.13422856	.61689120	.383	-.7311245	2.9995816
	3	1	.32730650	.61689120	.983	-1.5380465	2.1926595
		6	.97812925	.66631866	.595	-1.0366823	2.9929408
		9	1.26666557	.60202417	.261	-.5537326	3.0870637
		12	1.46153506	.71232461	.282	-.6923891	3.6154592
	6	1	-.65082275	.56314205	.775	-2.3536493	1.0520038
		3	-.97812925	.66631866	.595	-2.9929408	1.0366823
		9	.28853632	.54681561	.983	-1.3649224	1.9419951
		12	.48340581	.66631866	.948	-1.5314057	2.4982174
	9	1	-.93935907	.48536740	.335	-2.4070110	.5282928
		3	-1.26666557	.60202417	.261	-3.0870637	.5537326
		6	-.28853632	.54681561	.983	-1.9419951	1.3649224
		12	.19486948	.60202417	.997	-1.6255287	2.0152676
	12	1	-1.13422856	.61689120	.383	-2.9995816	.7311245
		3	-1.46153506	.71232461	.282	-3.6154592	.6923891
		6	-.48340581	.66631866	.948	-2.4982174	1.5314057
		9	-.19486948	.60202417	.997	-2.0152676	1.6255287

*. The mean difference is significant at the 0.05 level.

Distal Far Side

Table 5. Descriptive statistics of distal far side bone

		N	Mean	Std. Deviation	Std. Error	95% Confidence Interval for Mean		Minimum	Maximum
						Lower Bound	Upper Bound		
Phosphate Amidel	1	6	19.6215377	2.42709407	.99085700	17.0744587	22.1686167	16.86644	22.11910
	3	3	12.1442809	.22111790	.12766248	11.5949936	12.6935682	11.93377	12.37466
	6	4	17.1983595	4.30276323	2.15138161	10.3517030	24.0450159	13.62736	22.29231
	9	7	12.5565341	2.09385846	.79140411	10.6200380	14.4930302	8.84900	15.09963
	12	3	10.1830383	1.66201078	.95956237	6.0543747	14.3117020	8.92393	12.06689
	Total	23	14.8434939	4.26247323	.88878711	13.0002623	16.6867256	8.84900	22.29231
Carbonate Phosphate	1	6	.1907698	.02777870	.01134061	.1616178	.2199218	.16375	.21780
	3	3	.2938571	.01504069	.00868374	.2564940	.3312202	.28009	.30991
	6	4	.2047418	.02657079	.01328539	.1624618	.2470219	.17919	.23367
	9	7	.2157924	.05309357	.02006748	.1666890	.2648958	.17452	.32254
	12	3	.3154893	.09486290	.05476912	.0798368	.5511418	.24216	.42262
	Total	23	.2305292	.06349344	.01323930	.2030726	.2579858	.16375	.42262
Carbonate Amidel	1	6	3.6889783	.16600864	.06777274	3.5147630	3.8631937	3.51997	4.00192
	3	3	3.5676796	.16449704	.09497241	3.1590463	3.9763129	3.46600	3.75746
	6	4	3.4214622	.44637441	.22318720	2.7111809	4.1317434	2.99307	3.99152

Table 5 Continued

	9	7	2.5250734	.15534715	.05871570	2.3814013	2.6687456	2.30869	2.69396
	12	3	3.1333716	.83183054	.48025758	1.0669900	5.1997532	2.20657	3.81524
	Total	23	3.1999298	.58607665	.12220543	2.9464913	3.4533684	2.20657	4.00192
FWHMPhosphate	1	6	23.6596760	1.78449080	.72851532	21.7869678	25.5323842	21.98573	25.39008
	3	3	20.2446573	.18676270	.10782749	19.7807131	20.7086016	20.02901	20.35434
	6	4	22.7642903	1.35026778	.67513389	20.6157129	24.9128676	21.54283	24.64763
	9	7	21.5274926	.90254620	.34113040	20.6927766	22.3622086	20.45830	22.96361
	12	3	19.8308281	2.35499687	1.35965808	13.9806916	25.6809646	17.12273	21.39855
	Total	23	21.9101792	1.91929932	.40020157	21.0802119	22.7401465	17.12273	25.39008

Table 6. Analysis of Variance (ANOVA) output for distal far side bone

		Sum of Squares	df	Mean Square	F	Sig.
PhosphateAmideI	Between Groups	282.788	4	70.697	10.884	.000
	Within Groups	116.923	18	6.496		
	Total	399.711	22			
CarbonatePhosphate	Between Groups	.047	4	.012	5.154	.006
	Within Groups	.041	18	.002		
	Total	.089	22			
CarbonateAmideI	Between Groups	5.238	4	1.310	10.168	.000
	Within Groups	2.318	18	.129		
	Total	7.557	22			
FWHMPhosphate	Between Groups	43.601	4	10.900	5.240	.006
	Within Groups	37.441	18	2.080		
	Total	81.042	22			

Table 7. Multiple comparisons test using Tukey HSD for distal far side

Tukey HSD

Dependent Variable	(I) Month	(J) Month	Mean Difference (I-J)	Std. Error	Sig.	95% Confidence Interval	
						Lower Bound	Upper Bound
PhosphateAmideI	1	3	7.47725680*	1.80218269	.005	2.0278244	12.9266892
		6	2.42317824	1.64516018	.592	-2.5514502	7.3978067
		9	7.06500360*	1.41794975	.001	2.7774131	11.3525941
		12	9.43849937*	1.80218269	.000	3.9890670	14.8879318
	3	1	-7.47725680*	1.80218269	.005	-12.9266892	-2.0278244
		6	-5.05407856	1.94657978	.113	-10.9401383	.8319812
		9	-.41225320	1.75875021	.999	-5.7303547	4.9058483
		12	1.96124257	2.08098132	.877	-4.3312200	8.2537051
	6	1	-2.42317824	1.64516018	.592	-7.3978067	2.5514502
		3	5.05407856	1.94657978	.113	-.8319812	10.9401383
		9	4.64182536	1.59746421	.063	-.1885802	9.4722309
		12	7.01532113*	1.94657978	.015	1.1292614	12.9013809
	9	1	-7.06500360*	1.41794975	.001	-11.3525941	-2.7774131
		3	.41225320	1.75875021	.999	-4.9058483	5.7303547
		6	-4.64182536	1.59746421	.063	-9.4722309	.1885802
		12	2.37349577	1.75875021	.665	-2.9446057	7.6915973

Table 7 Continued

	12	1	-9.43849937*	1.80218269	.000	-14.8879318	-3.9890670
		3	-1.96124257	2.08098132	.877	-8.2537051	4.3312200
		6	-7.01532113*	1.94657978	.015	-12.9013809	-1.1292614
		9	-2.37349577	1.75875021	.665	-7.6915973	2.9446057
CarbonatePhosphate	1	3	-.10308728*	.03388717	.048	-.2055552	-.0006194
		6	-.01397204	.03093461	.991	-.1075120	.0795679
		9	-.02502259	.02666228	.878	-.1056439	.0555987
		12	-.12471944*	.03388717	.013	-.2271873	-.0222516
	3	1	.10308728*	.03388717	.048	.0006194	.2055552
		6	.08911524	.03660233	.151	-.0215627	.1997932
		9	.07806469	.03307049	.172	-.0219337	.1780631
		12	-.02163216	.03912953	.980	-.1399519	.0966876
	6	1	.01397204	.03093461	.991	-.0795679	.1075120
		3	-.08911524	.03660233	.151	-.1997932	.0215627
		9	-.01105055	.03003777	.996	-.1018786	.0797775
		12	-.11074740*	.03660233	.050	-.2214254	-.0000694
	9	1	.02502259	.02666228	.878	-.0555987	.1056439
		3	-.07806469	.03307049	.172	-.1780631	.0219337
		6	.01105055	.03003777	.996	-.0797775	.1018786
		12	-.09969686	.03307049	.051	-.1996953	.0003016
	12	1	.12471944*	.03388717	.013	.0222516	.2271873
		3	.02163216	.03912953	.980	-.0966876	.1399519
		6	.11074740*	.03660233	.050	.0000694	.2214254
		9	.09969686	.03307049	.051	-.0003016	.1996953
CarbonateAmideI	1	3	.12129873	.25376847	.988	-.6460453	.8886428
		6	.26751618	.23165786	.776	-.4329699	.9680022
		9	1.16390489*	.19966397	.000	.5601618	1.7676480
		12	.55560676	.25376847	.228	-.2117373	1.3229508
	3	1	-.12129873	.25376847	.988	-.8886428	.6460453
		6	.14621745	.27410128	.983	-.6826088	.9750437
		9	1.04260617*	.24765267	.004	.2937551	1.7914573
		12	.43430803	.29302659	.586	-.4517445	1.3203606

Table 7 Continued

	6	1	-.26751618	.23165786	.776	-.9680022	.4329699
		3	-.14621745	.27410128	.983	-.9750437	.6826088
		9	.89638872*	.22494171	.007	.2162109	1.5765665
		12	.28809058	.27410128	.828	-.5407357	1.1169169
	9	1	-1.16390489*	.19966397	.000	-1.7676480	-.5601618
		3	-1.04260617*	.24765267	.004	-1.7914573	-.2937551
		6	-.89638872*	.22494171	.007	-1.5765665	-.2162109
		12	-.60829814	.24765267	.145	-1.3571492	.1405530
	12	1	-.55560676	.25376847	.228	-1.3229508	.2117373
		3	-.43430803	.29302659	.586	-1.3203606	.4517445
		6	-.28809058	.27410128	.828	-1.1169169	.5407357
		9	.60829814	.24765267	.145	-.1405530	1.3571492
FWHMPhosphate	1	3	3.41501867*	1.01981786	.026	.3312977	6.4987396
		6	.89538575	.93096208	.869	-1.9196535	3.7104250
		9	2.13218341	.80238841	.101	-.2940753	4.5584421
		12	3.82884790*	1.01981786	.011	.7451269	6.9125689
	3	1	-3.41501867*	1.01981786	.026	-6.4987396	-.3312977
		6	-2.51963292	1.10152919	.194	-5.8504322	.8111664
		9	-1.28283526	.99524033	.701	-4.2922388	1.7265682
		12	.41382923	1.17758424	.996	-3.1469450	3.9746035
	6	1	-.89538575	.93096208	.869	-3.7104250	1.9196535
		3	2.51963292	1.10152919	.194	-.8111664	5.8504322
		9	1.23679766	.90397192	.654	-1.4966288	3.9702241
		12	2.93346215	1.10152919	.100	-.3973372	6.2642615
	9	1	-2.13218341	.80238841	.101	-4.5584421	.2940753
		3	1.28283526	.99524033	.701	-1.7265682	4.2922388
		6	-1.23679766	.90397192	.654	-3.9702241	1.4966288
		12	1.69666449	.99524033	.456	-1.3127390	4.7060680

Table 7 Continued

12	1	-3.82884790*	1.01981786	.011	-6.9125689	-.7451269
	3	-.41382923	1.17758424	.996	-3.9746035	3.1469450
	6	-2.93346215	1.10152919	.100	-6.2642615	.3973372
	9	-1.69666449	.99524033	.456	-4.7060680	1.3127390

*. The mean difference is significant at the 0.05 level.

Proximal Near Side

Table 8. Descriptive statistics of proximal near side bone

						95% Confidence Interval for Mean			
		N	Mean	Std. Deviation	Std. Error	Lower Bound	Upper Bound	Minimum	Maximum
PhosphateAmidel	1	6	14.9552840	3.98786193	1.62803782	10.7702796	19.1402884	12.52798	22.95669
	3	3	15.5791845	.12501687	.07217853	15.2686254	15.8897436	15.44326	15.68925
	6	4	14.1068016	1.76426072	.88213036	11.2994691	16.9141341	12.69895	16.67093
	9	7	11.4243485	3.23187541	1.22153409	8.4353623	14.4133348	7.59713	16.68106
	12	3	10.2315585	2.13344337	1.23174410	4.9317913	15.5313256	8.56821	12.63693
	Total	23	13.1983295	3.35694583	.69997159	11.7466773	14.6499818	7.59713	22.95669
CarbonatePhosphate	1	6	.2606862	.00418858	.00170998	.2562905	.2650818	.25618	.26830
	3	3	.2238248	.00553160	.00319367	.2100835	.2375661	.21772	.22850
	6	4	.2287252	.00986550	.00493275	.2130270	.2444234	.21472	.23790
	9	7	.2472515	.07882932	.02979468	.1743466	.3201565	.15630	.35282
	12	3	.2235836	.03737305	.02157734	.1307437	.3164234	.19126	.26451
	Total	23	.2413915	.04548313	.00948389	.2217231	.2610598	.15630	.35282
CarbonateAmidel	1	6	3.8935196	1.00901444	.41192842	2.8346239	4.9524153	3.26280	5.91580
	3	3	3.4865845	.06166364	.03560152	3.3334035	3.6397654	3.41581	3.52873
	6	4	3.0389637	.43993165	.21996582	2.3389343	3.7389931	2.45342	3.52103

Table 8 Continued

	9	7	2.4271242	.37151521	.14041955	2.0835299	2.7707184	1.96461	3.07339
	12	3	2.2911275	.37825184	.21838380	1.3514978	3.2307571	2.00133	2.71902
	Total	23	3.0365208	.85476807	.17823146	2.6668913	3.4061502	1.96461	5.91580
FWHMPhosphate	1	6	21.6292005	.12461325	.05087314	21.4984269	21.7599741	21.46070	21.81464
	3	3	25.3320440	.24722239	.14273391	24.7179095	25.9461785	25.04804	25.49901
	6	4	22.4105505	1.61303177	.80651589	19.8438570	24.9772440	21.12505	24.68146
	9	7	21.4035103	1.53725585	.58102810	19.9817858	22.8252349	20.25695	24.73609
	12	3	18.9929242	1.55636006	.89856490	15.1267114	22.8591369	17.19731	19.95460
	Total	23	21.8355166	2.03192148	.42368492	20.9568478	22.7141853	17.19731	25.49901

Table 9. Analysis of Variance (ANOVA) output for proximal near side

		Sum of Squares	df	Mean Square	F	Sig.
PhosphateAmideI	Between Groups	87.262	4	21.816	2.444	.084
	Within Groups	160.658	18	8.925		
	Total	247.920	22			
CarbonatePhosphate	Between Groups	.005	4	.001	.555	.698
	Within Groups	.041	18	.002		
	Total	.046	22			
CarbonateAmideI	Between Groups	9.281	4	2.320	6.148	.003
	Within Groups	6.793	18	.377		
	Total	16.074	22			
FWHMPhosphate	Between Groups	63.803	4	15.951	10.622	.000
	Within Groups	27.029	18	1.502		
	Total	90.832	22			

Table 10. Multiple comparisons test using Tukey HSD for proximal near side

Tukey HSD

Dependent Variable	(I) Month	(J) Month	Mean Difference (I-J)	Std. Error	Sig.	95% Confidence Interval	
						Lower Bound	Upper Bound
PhosphateAmideI	1	3	-.62390051	2.11251294	.998	-7.0117082	5.7639072
		6	.84848238	1.92845165	.992	-4.9827616	6.6797264
		9	3.53093546	1.66211629	.253	-1.4949648	8.5568357
		12	4.72372554	2.11251294	.211	-1.6640822	11.1115333
	3	1	.62390051	2.11251294	.998	-5.7639072	7.0117082
		6	1.47238289	2.28177477	.965	-5.4272380	8.3720038
		9	4.15483597	2.06160153	.298	-2.0790261	10.3886980
		12	5.34762605	2.43931983	.227	-2.0283790	12.7236311
	6	1	-.84848238	1.92845165	.992	-6.6797264	4.9827616
		3	-1.47238289	2.28177477	.965	-8.3720038	5.4272380
		9	2.68245308	1.87254258	.616	-2.9797333	8.3446394
		12	3.87524316	2.28177477	.459	-3.0243778	10.7748641
	9	1	-3.53093546	1.66211629	.253	-8.5568357	1.4949648
		3	-4.15483597	2.06160153	.298	-10.3886980	2.0790261
		6	-2.68245308	1.87254258	.616	-8.3446394	2.9797333
		12	1.19279008	2.06160153	.977	-5.0410719	7.4266521
	12	1	-4.72372554	2.11251294	.211	-11.1115333	1.6640822

Table 10 Continued

		3	-5.34762605	2.43931983	.227	-12.7236311	2.0283790
		6	-3.87524316	2.28177477	.459	-10.7748641	3.0243778
		9	-1.19279008	2.06160153	.977	-7.4266521	5.0410719
CarbonatePhosphate	1	3	.03686138	.03354879	.805	-.0645833	.1383061
		6	.03196102	.03062571	.832	-.0606449	.1245669
		9	.01343467	.02639604	.985	-.0663816	.0932509
		12	.03710263	.03354879	.801	-.0643421	.1385473
	3	1	-.03686138	.03354879	.805	-.1383061	.0645833
		6	-.00490036	.03623683	1.000	-.1144731	.1046724
		9	-.02342671	.03274026	.950	-.1224266	.0755732
		12	.00024125	.03873880	1.000	-.1168970	.1173795
	6	1	-.03196102	.03062571	.832	-.1245669	.0606449
		3	.00490036	.03623683	1.000	-.1046724	.1144731
		9	-.01852635	.02973782	.969	-.1084474	.0713947
		12	.00514161	.03623683	1.000	-.1044312	.1147144
	9	1	-.01343467	.02639604	.985	-.0932509	.0663816
		3	.02342671	.03274026	.950	-.0755732	.1224266
		6	.01852635	.02973782	.969	-.0713947	.1084474
		12	.02366796	.03274026	.948	-.0753319	.1226678
	12	1	-.03710263	.03354879	.801	-.1385473	.0643421
		3	-.00024125	.03873880	1.000	-.1173795	.1168970
		6	-.00514161	.03623683	1.000	-.1147144	.1044312
		9	-.02366796	.03274026	.948	-.1226678	.0753319
CarbonateAmideI	1	3	.40693511	.43439183	.879	-.9065771	1.7204473
		6	.85455590	.39654367	.241	-.3445112	2.0536230
		9	1.46639543*	.34177766	.004	.4329296	2.4998613
		12	1.60239211*	.43439183	.013	.2888799	2.9159043
	3	1	-.40693511	.43439183	.879	-1.7204473	.9065771
		6	.44762079	.46919680	.872	-.9711345	1.8663761
		9	1.05946031	.42392301	.135	-.2223963	2.3413169
		12	1.19545700	.50159248	.165	-.3212562	2.7121702
	6	1	-.85455590	.39654367	.241	-2.0536230	.3445112
		3	-.44762079	.46919680	.872	-1.8663761	.9711345

Table 10 Continued

		9	.61183953	.38504720	.522	-.5524646	1.7761436
		12	.74783621	.46919680	.520	-.6709191	2.1665915
	9	1	-1.46639543*	.34177766	.004	-2.4998613	-.4329296
		3	-1.05946031	.42392301	.135	-2.3413169	.2223963
		6	-.61183953	.38504720	.522	-1.7761436	.5524646
		12	.13599669	.42392301	.997	-1.1458599	1.4178533
	12	1	-1.60239211*	.43439183	.013	-2.9159043	-.2888799
		3	-1.19545700	.50159248	.165	-2.7121702	.3212562
		6	-.74783621	.46919680	.520	-2.1665915	.6709191
		9	-.13599669	.42392301	.997	-1.4178533	1.1458599
FWHMPhosphate	1	3	-3.70284350*	.86648942	.004	-6.3229306	-1.0827564
		6	-.78134998	.79099301	.857	-3.1731513	1.6104513
		9	.22569019	.68175023	.997	-1.8357833	2.2871637
		12	2.63627634*	.86648942	.048	.0161893	5.2563634
	3	1	3.70284350*	.86648942	.004	1.0827564	6.3229306
		6	2.92149352*	.93591555	.041	.0914760	5.7515110
		9	3.92853369*	.84560709	.002	1.3715905	6.4854769
		12	6.33911984*	1.00053581	.000	3.3137039	9.3645358
	6	1	.78134998	.79099301	.857	-1.6104513	3.1731513
		3	-2.92149352*	.93591555	.041	-5.7515110	-.0914760
		9	1.00704016	.76806078	.688	-1.3154188	3.3294991
		12	3.41762632*	.93591555	.014	.5876088	6.2476438
	9	1	-.22569019	.68175023	.997	-2.2871637	1.8357833
		3	-3.92853369*	.84560709	.002	-6.4854769	-1.3715905
		6	-1.00704016	.76806078	.688	-3.3294991	1.3154188
		12	2.41058615	.84560709	.070	-.1463570	4.9675293
	12	1	-2.63627634*	.86648942	.048	-5.2563634	-.0161893
		3	-6.33911984*	1.00053581	.000	-9.3645358	-3.3137039
		6	-3.41762632*	.93591555	.014	-6.2476438	-.5876088
		9	-2.41058615	.84560709	.070	-4.9675293	.1463570

*. The mean difference is significant at the 0.05 level.

Proximal Far Side

Table 11. Descriptive statistics of proximal far side bone

		N	Mean	Std. Deviation	Std. Error	95% Confidence Interval for Mean		Minimum	Maximum
						Lower Bound	Upper Bound		
Phosphate Amidel	1	5	17.8916220	6.87186434	3.07319116	9.3590754	26.4241686	11.13803	27.98084
	3	2	17.7249595	.02543420	.01798470	17.4964423	17.9534767	17.70697	17.74294
	6	4	13.7277865	4.82085915	2.41042957	6.0567238	21.3988492	8.26674	19.58657
	9	7	12.0813756	5.42412824	2.05012777	7.0648937	17.0978575	6.68588	22.30053
	12	3	17.6151485	7.08536747	4.09073882	.0141200	35.2161771	10.03063	24.06424
	Total	21	15.1063929	5.82488121	1.27109329	12.4549387	17.7578470	6.68588	27.98084
Carbonate Phosphate	1	5	.2638186	.01603719	.00717205	.2439057	.2837314	.24465	.28245
	3	2	.2047828	.00103437	.00073141	.1954893	.2140763	.20405	.20551
	6	4	.2551601	.06410742	.03205371	.1531509	.3571693	.19684	.34498
	9	7	.2775991	.13136713	.04965211	.1561048	.3990934	.17163	.54047
	12	3	.1890544	.02427189	.01401338	.1287597	.2493491	.16821	.21570
	Total	21	.2504598	.08357703	.01823800	.2124160	.2885036	.16821	.54047
Carbonate Amidel	1	5	4.6669032	1.68950223	.75556837	2.5691091	6.7646973	3.14590	7.34462
	3	2	3.6297537	.01312571	.00928128	3.5118239	3.7476835	3.62047	3.63903
	6	4	3.1581024	.50554489	.25277244	2.3536677	3.9625372	2.72123	3.74155
	9	7	2.7296184	.52446200	.19822800	2.2445719	3.2146648	2.19635	3.82153

Table 11 Continued

	12	3	3.2203608	1.04939449	.60586819	.6135204	5.8272012	2.04219	4.05473
	Total	21	3.4283259	1.17533149	.25647836	2.8933214	3.9633304	2.04219	7.34462
FWHM Phosphate	1	5	21.2752604	.66350253	.29672735	20.4514132	22.0991076	20.47483	21.85154
	3	2	24.2617970	.07913091	.05595400	23.5508340	24.9727600	24.20584	24.31775
	6	4	21.9971890	1.97741120	.98870560	18.8506865	25.1436915	20.18432	24.80494
	9	7	21.1099307	1.18709351	.44867917	20.0120523	22.2078091	20.06460	23.32507
	12	3	19.8308281	2.35499687	1.35965808	13.9806916	25.6809646	17.12273	21.39855
	Total	21	21.4357453	1.71577955	.37441379	20.6547318	22.2167588	17.12273	24.80494

Table 12. Analysis of variance (ANOVA) output for proximal far side

		Sum of Squares	df	Mean Square	F	Sig.
PhosphateAmideI	Between Groups	143.040	4	35.760	1.068	.404
	Within Groups	535.545	16	33.472		
	Total	678.585	20			
CarbonatePhosphate	Between Groups	.022	4	.005	.732	.583
	Within Groups	.118	16	.007		
	Total	.140	20			
CarbonateAmideI	Between Groups	11.591	4	2.898	2.891	.056
	Within Groups	16.037	16	1.002		
	Total	27.628	20			
FWHMPhosphate	Between Groups	25.833	4	6.458	3.127	.044
	Within Groups	33.045	16	2.065		
	Total	58.878	20			

Table 13. Multiple comparisons test using Tukey HSD for proximal far side

Tukey HSD

Dependent Variable	(I) Month	(J) Month	Mean Difference (I-J)	Std. Error	Sig.	95% Confidence Interval	
						Lower Bound	Upper Bound
PhosphateAmideI	1	3	.16666249	4.84046259	1.000	-14.6629318	14.9962568
		6	4.16383550	3.88100413	.818	-7.7262919	16.0539629
		9	5.81024639	3.38761813	.453	-4.5683077	16.1888004
		12	.27647348	4.22510213	1.000	-12.6678577	13.2208046
	3	1	-.16666249	4.84046259	1.000	-14.9962568	14.6629318
		6	3.99717301	5.01035478	.927	-11.3529154	19.3472615
		9	5.64358391	4.63868716	.742	-8.5678365	19.8550043
		12	.10981100	5.28137767	1.000	-16.0706029	16.2902249
	6	1	-4.16383550	3.88100413	.818	-16.0539629	7.7262919
		3	-3.99717301	5.01035478	.927	-19.3472615	11.3529154
		9	1.64641090	3.62622856	.990	-9.4631675	12.7559893
		12	-3.88736202	4.41871758	.900	-17.4248676	9.6501435
	9	1	-5.81024639	3.38761813	.453	-16.1888004	4.5683077
		3	-5.64358391	4.63868716	.742	-19.8550043	8.5678365
		6	-1.64641090	3.62622856	.990	-12.7559893	9.4631675
		12	-5.53377291	3.99234625	.645	-17.7650162	6.6974703
	12	1	-.27647348	4.22510213	1.000	-13.2208046	12.6678577
		3	-.10981100	5.28137767	1.000	-16.2902249	16.0706029
		6	3.88736202	4.41871758	.900	-9.6501435	17.4248676
		9	5.53377291	3.99234625	.645	-6.6974703	17.7650162
CarbonatePhosphate	1	3	.05903575	.07187529	.920	-.1611666	.2792381
		6	.00865848	.05762844	1.000	-.1678962	.1852132
		9	-.01378057	.05030222	.999	-.1678901	.1403290
		12	.07476416	.06273789	.756	-.1174442	.2669725
	3	1	-.05903575	.07187529	.920	-.2792381	.1611666
		6	-.05037728	.07439799	.959	-.2783084	.1775538
		9	-.07281632	.06887916	.825	-.2838395	.1382069
		12	.01572840	.07842237	1.000	-.2245321	.2559889
	6	1	-.00865848	.05762844	1.000	-.1852132	.1678962
		3	.05037728	.07439799	.959	-.1775538	.2783084
		9	-.02243905	.05384531	.993	-.1874035	.1425254
		12	.06610568	.06561286	.848	-.1349107	.2671220
	9	1	.01378057	.05030222	.999	-.1403290	.1678901

Table 13 Continued

		3	.07281632	.06887916	.825	-.1382069	.2838395
		6	.02243905	.05384531	.993	-.1425254	.1874035
		12	.08854473	.05928174	.581	-.0930751	.2701646
	12	1	-.07476416	.06273789	.756	-.2669725	.1174442
		3	-.01572840	.07842237	1.000	-.2559889	.2245321
		6	-.06610568	.06561286	.848	-.2671220	.1349107
		9	-.08854473	.05928174	.581	-.2701646	.0930751
CarbonateAmideI	1	3	1.03714955	.83763705	.730	-1.5290964	3.6033955
		6	1.50880078	.67160375	.213	-.5487735	3.5663750
		9	1.93728484*	.58622382	.031	.1412868	3.7332829
		12	1.44654240	.73114956	.319	-.7934607	3.6865455
	3	1	-1.03714955	.83763705	.730	-3.6033955	1.5290964
		6	.47165123	.86703672	.981	-2.1846657	3.1279682
		9	.90013528	.80272002	.793	-1.5591363	3.3594069
		12	.40939285	.91393695	.991	-2.3906111	3.2093968
	6	1	-1.50880078	.67160375	.213	-3.5663750	.5487735
		3	-.47165123	.86703672	.981	-3.1279682	2.1846657
		9	.42848406	.62751511	.957	-1.4940170	2.3509851
		12	-.06225838	.76465451	1.000	-2.4049097	2.2803930
	9	1	-1.93728484*	.58622382	.031	-3.7332829	-.1412868
		3	-.90013528	.80272002	.793	-3.3594069	1.5591363
		6	-.42848406	.62751511	.957	-2.3509851	1.4940170
		12	-.49074243	.69087139	.951	-2.6073464	1.6258616
	12	1	-1.44654240	.73114956	.319	-3.6865455	.7934607
		3	-.40939285	.91393695	.991	-3.2093968	2.3906111
		6	.06225838	.76465451	1.000	-2.2803930	2.4049097
		9	.49074244	.69087139	.951	-1.6258616	2.6073464
FWHMPhosphate	1	3	-2.98653660	1.20237746	.144	-6.6702279	.6971547
		6	-.72192860	.96404668	.941	-3.6754523	2.2315951
		9	.16532973	.84148893	1.000	-2.4127172	2.7433766
		12	1.44443230	1.04952109	.650	-1.7709571	4.6598217
	3	1	2.98653660	1.20237746	.144	-.6971547	6.6702279
		6	2.26460800	1.24457892	.397	-1.5483748	6.0775908
		9	3.15186633	1.15225618	.092	-.3782698	6.6820024
		12	4.43096890*	1.31190137	.027	.4117322	8.4502056
	6	1	.72192860	.96404668	.941	-2.2315951	3.6754523

Table 13 Continued

		3	-2.26460800	1.24457892	.397	-6.0775908	1.5483748
		9	.88725833	.90076009	.858	-1.8723760	3.6468927
		12	2.16636090	1.09761543	.321	-1.1963738	5.5290956
	9	1	-.16532973	.84148893	1.000	-2.7433766	2.4127172
		3	-3.15186633	1.15225618	.092	-6.6820024	.3782698
		6	-.88725833	.90076009	.858	-3.6468927	1.8723760
		12	1.27910256	.99170422	.701	-1.7591548	4.3173600
	12	1	-1.44443230	1.04952109	.650	-4.6598217	1.7709571
		3	-4.43096890*	1.31190137	.027	-8.4502056	-.4117322
		6	-2.16636090	1.09761543	.321	-5.5290956	1.1963738
		9	-1.27910256	.99170422	.701	-4.3173600	1.7591548

*. The mean difference is significant at the 0.05 level.

VITA

Alyssa Rose Daniel was born to Chris and Donna Daniel and grew up in Davenport, Iowa. Alyssa attended Davenport Assumption High School and graduated in May 2013. She then attended Saint Ambrose University, where she earned a Bachelor of Science degree in Chemistry and minors in Biology as well as Forensic Science and Justice and graduated in 2017. During her time at Saint Ambrose University, she participated in several research experiences, including a summer undergraduate research experience at the University of Iowa. Alyssa was accepted into the graduate program at the University of Tennessee, Knoxville, where she worked in Dr. Bhavya Sharma’s lab and studied Raman spectroscopic applications to forensic science.